Molecular dynamics of tryptophan in ribonuclease-T1
II. Correlations with fluorescence

Paul H. Axelsen and Franklyn G. Prendergast
Department of Biochemistry and Molecular Biology, Mayo Foundation, Rochester, Minnesota 55905

ABSTRACT The interactions of tryptophan-59 (TRP-59) and its protein environment in ribonuclease-T1 (RNAse-T1) were examined in a 50-ps molecular dynamics simulation. The simulation used was previously shown to demonstrate a fluorescence anisotropy decay that closely agreed with the experimentally determined limiting anistropy for RNAse-T1 (Axelsen, P. H., C. Haydock, and F. G. Prendergast. 1988. *Biophys. J.* 54:249–258). Further characterization of TRP-59 side chain dynamics and its protein environment has now been completed and correlated to other photophysical properties of this protein. Angular fluctuations of the side chain occur at rates of 1–10 cycles/ps and are limited to ±0.3 radians in all directions. Side chain motions are primarily limited by nonpolar collisions, although most side chain atoms have some collisional contact with polar atoms in the adjacent protein matrix or water. The steric relationship between PRO-39 and TRP-59 changes abruptly at 16 ps into the simulation. Two types of interaction with water are observed. First, a structural water appears to H-bond with the >N—H group of TRP-59. Second, water frequently contacts the six-atom ring. The electrostatic field experienced by the TRP-59 rings appears to be relatively constant and featureless regardless of ring orientation. We make the following inferences from our data: The fluorescent emission of TRP-59 may be red-shifted relative to TRP in nonpolar solvents either as a result of specific interactions with the structural water or relaxations of proximal bulk water and polar protein moieties. The quenching efficiency of polar interactions with TRP-59 must be extremely low given their frequency and the high quantum yield of RNAse-T1. This low efficiency may be due to restricted and unfavorable interaction geometries. PRO-39 is located near two titratable HIS residues in RNAse-T1 and may be involved in pH-dependent fluorescence phenomena by virtue of a metastable interaction with TRP-59. The interaction of bulk water with TRP-59 illustrates features of the gated transition state model for transient exposure to exogenously added collisional quenching agents. The restrictive environment of TRP-59 suggests that extrinsic quenching can only occur via interactions with the edge of the indole six-atom ring and that the efficiency of a quencher in a protein environment is likely to be a function of molecular symmetry.

INTRODUCTION

All measurable photophysical properties of the tryptophan (TRP) fluorophore are susceptible to physicochemical perturbation. As a consequence, information about TRP environments within a protein is encrypted within protein fluorescence emissions. In principle, TRP should be useful as a probe of protein structure and dynamics, particularly when there is only one TRP residue in the protein to which the fluorescence emission may be assigned. In practice, however, decrypting protein fluorescence emissions into accurate information about TRP environments is problematic. For example, there is no straightforward correlation between spectral position and location of a TRP side chain within a protein. The dependence of TRP fluorescence on solvent character is complex (Creed, 1984; Demchenko, 1986), and consequently empirical rules for assigning the location of a TRP side chain within a protein on the basis of solvent accessibility are at best only grossly approximate (Burstein et al., 1973). We also cannot readily interpret fluorescence lifetimes which range, for example, from <0.5 ns in scorpion neurotoxin (var. 3) to >7.0 ns in phospholipase A2 (Beechem and Brand, 1985; Alcala et al., 1987*b*). Fluorescence lifetimes are often resolvable into two or more quasi-unique components which do not have clear structural correlations and whose relative contributions vary unpredictably with factors such as temperature and pH (Beechem and Brand, 1985; Gryczynski et al., 1988). In sum, our basic understanding of protein fluorescence has advanced slowly in comparison to our appreciation for its complexity (as anticipated by Longworth, 1971), despite the wide-ranging and increasingly apparent utility of protein fluorescence.

Ideally, we would like to explain TRP fluorescence in terms of its intrinsic photophysical properties and specific protein-solvent influences. Without question, protein crystal structures are of enormous help in this regard. Yet, crystal structures are not without limitations, and can be misleading at times. For example, crystal coordi-

0006-3495/89/07/43/24 $2.00

nates are in fact average atomic positions (Ringe and Petsko, 1985), and as a consequence, may represent an improbable set of atomic relationships for a given instant in time. The interactions between solvent and residues on the protein surface are often ambiguous, and not infrequently, entire side chains or even multiple residue segments of the protein are disordered. Even when "crystal waters" can be localized, hydrogen atom positions are usually not determinable and the presence of hydrogen bonds is therefore deduced rather than observed. Protein crystals are difficult to study spectroscopically, and we usually do not know the extent to which crystal and solution structures for a protein differ. Finally, crystal data yield an essentially static image of a protein. Temperature factors, to the extent that they are a function of atomic motion, are subject to an isotropic approximation and thus do not assist us in understanding the anisotropic aspects of atomic motions.

In view of these limitations, it is logical to pursue computer simulations of protein dynamics. Because the initial structure for such simulations is generally derived from crystallographic data, a molecular dynamics trajectory is an extrapolation from the crystal structure. These extrapolations enable the study of plausible relationships between fluorophore and protein matrix that would otherwise not be evident in static representations of the crystal structure. It is important to recognize that simulations of protein dynamics generally span time intervals <1 ns and thus, such simulations can at best sample a minute fraction of the total conformational space available to a protein. Nevertheless, significant motions do occur on the time scale which is presently accessible to simulation, and several interesting studies correlating fluorescence data and molecular dynamics simulations have appeared (Henry and Hochstrasser, 1987; Chen et al., 1988*b*; MacKerrel et al., 1987, 1988). Furthermore, it is clear that protein fluorescence, though it may persist in intensity for several nanoseconds, is primarily governed by subnanosecond events. Photoexcitation, for example, occurs in <1 fs (the Frank-Condon principle). Time-dependent depolarization appears to be a function of innumerable interatomic collisions, all occurring on the femtosecond-picosecond time scale (Chen et al., 1988*a*). Quenching, particularly in the case of fluorophores rendered photoemissively silent within their protein environment, must be effective on a time scale several orders of magnitude smaller than the fluorescence lifetime. In addition, transient phenomena are observed at subnanosecond time intervals and high quencher concentrations and are presumably due to the existence of fluorophore-quencher pairs capable of interacting faster than diffusion-limited rates (Lakowicz et al., 1987).

The enzyme RNAse-T1 was chosen for this study on account of several unusual and interesting features: a high limiting anisotropy (Lackowicz et al., 1983; Eftink, 1983), a blue-shifted and semistructured emission spectrum, and a differential susceptibility of its fluorescence to quenching agents (James et al., 1985). These characteristics suggested to us that (*a*) simulated anisotropy decay in RNAse-T1 may be directly compared with experimental data, (*b*) steric relationships between the TRP residue and the protein will be relatively fixed and thus simpler to characterize, (*c*) one or more intrinsic protein moieties capable of perturbing indole might be identified, and (*d*) the protein surface topography and protein matrix dynamics may help explain the behavior of quenchers in the vicinity of the TRP.

In an earlier paper, we found excellent agreement between the simulation-derived fluorescence anisotropy decay of TRP-59 and experimental determinations of its limiting anisotropy, illustrating in this case how fluorescence data can yield insight into the validity of a molecular dynamics simulation (Axelsen et al., 1988). In the work described below, we have examined the utility of molecular dynamics in the interpretation of fluorescence data. We find that simulations of molecular dynamics are highly effective stimuli to the generation of hypotheses concerning the origin and interpretation of fluorescence. Importantly, these hypotheses should be testable in many cases through the study of specifically mutated proteins, and simulations greatly facilitate the design of such proteins.

METHODS

The dynamics trajectory used for the analysis below has been described previously (Axelsen et al., 1988). Briefly, a subset of atoms from the crystal structure of RNAse-T1 (Heinemann and Saenger, 1982) was propagated for 50 ps within a stochastic boundary at 300°K. The boundary had been positioned such that the two major secondary structures adjacent to TRP-59 (helix 12-29 and loop 60-77) were entirely within the boundary. The system consisted of 462 explicitly modeled hydrogens, 536 heavier atoms, and 204 TIP3 water models for a total of 1,610 atoms. References to specific water molecules are made using the residue number of the most closely corresponding crystal water in the data deposited with the Brookhaven Protein Data Bank (Bernstein et al., 1977) when the residue number is ≤201. Waters with residue numbers >201 were numbered arbitrarily. Coordinates were saved at 0.02-ps intervals, yielding a total of 2,500 discrete coordinate sets for the 50-ps trajectory.

Analysis was performed using locally augmented versions of CHARMM (Brooks et al., 1983; version 20 distributed by Polygen Corp., Waltham, MA). Vector graphics were produced using HYDRA (Polygen Corp.) on a PS330 vector graphics system (Evans & Sutherland, Salt Lake City, UT) and a Microvax II (Digital Equipment Co., Waltham, MA). Dot surfaces for graphics were generated using MS (Connolly, 1983) using atomic radii that corresponded to zero interaction energy for the corresponding atom in CHARMM. This was generally the R_{min} value for the VDW interaction energy scaled by 0.89, and a probe of 1.0 Å was used so that it entered the space available to hydrogen atoms. Numerical values for solvent accessible surface areas

were calculated using the algorithm of Lee and Richards (1971). Plots were generated using PLT2 by States, D., et al. (unpublished) or a commercially available contouring package (Prevision Visuals Inc., Boulder, CO). The crystal structures for azurin (Adman and Jensen, 1981; from *P. aeruginosa*) and nuclease (Cotton et al., 1979; from *S. aureus*) were also obtained from the Brookhaven Protein Data Bank.

RESULTS

I. Correlation between temperature factors and fluctuations

In general, a crystallographically-derived temperature factor, B, should be greater than $8\pi^2\langle x^2\rangle$, where $\langle x^2\rangle$ is the mean-squared fluctuation of an atom from its average position in a molecular dynamics simulation. This is to be expected because static disorder in the crystal lattice will exaggerate temperature factors (Ringe and Petsko, 1985) and dynamics simulations may underestimate fluctuations due to limited sampling of conformational space. Fig. 1 *a* illustrates this trend for all atoms within the 14 Å reaction zone.

The finding of some atoms in which $B < 8\pi^2\langle x^2\rangle$ (left of an $x = y$ line in Fig. 1 *a*) is of interest. Our first expectation was that such atoms would be found within the protein crystal at points of intermolecular contact. As shown in Fig. 1 *b* this was not the case and atoms which are involved in intermolecular contacts either directly or via hydrogen-bonded water (Arni et al., 1987) are found entirely in the $B > 8\pi^2\langle x^2\rangle$ region. Graphical inspection of atoms in the $B < 8\pi^2\langle x^2\rangle$ set of Fig. 1 *a* reveals that most are side chain atoms, and that several of these comprise atom pairs which are symmetrically related to an X_1 or X_2 axis (see Table 1). Thus, these data suggest that rotations about certain X_1 or X_2 bonds are greater in our simulation than in the crystal. However, this conclusion must be qualified because the motions of an atom pair rotating about a specific bond are inherently anisotropic. Therefore, the fluctuations which appear to be anomalous may only be so on account of the isotropic approximation used in calculating temperature factors.

Fig. 1 *c* identifies atoms whose average position is within 8 Å of the reaction zone center where any artifacts due to the boundary and buffer region constraints should be minimized. Curiously, most of these atoms for which $B < 8\pi^2\langle x^2\rangle$ are adjacent to one or more atoms of

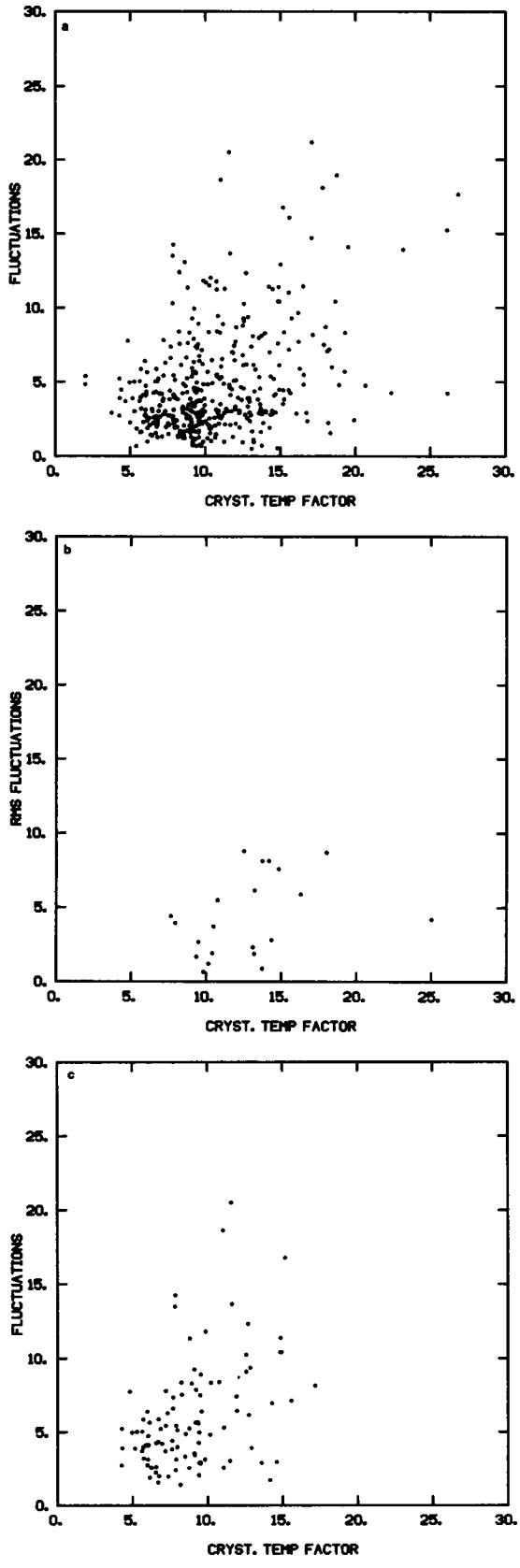

FIGURE 1 The relationship between crystallographic temperature factors and mean square displacements from average position for nonhydrogen atoms in the simulation. Fluctuations are plotted as $8\pi^2\langle x^2\rangle$ in units of Å^2 where $\langle x^2\rangle$ is the mean square fluctuation about an average position during the last 25 ps of the simulation. (*a*) All nonhydrogen atoms; (*b*) atoms at points of crystal contact, (*c*) atoms with 8 Å of the center of the boundary.

TABLE 1 Atoms in the simulation for which $B < 8\pi^2\langle x^2\rangle$ where B is the crystallographic temperature factor and $\langle x^2\rangle$ is the mean square fluctuation of the atom about its average position during the simulation

Atom	ID	$8\pi^2\langle x^2\rangle$	B
TYR 11	Oη	4.48	4.39
ASP 15	Cγ	11.69	10.03
*ASP 15	Oδ1	53.42	9.52
*ASP 15	Oδ2	11.49	10.26
THR 18	Cγ2	11.23	10.75
ALA 19	Cβ	4.98	4.95
ALA 21	Cβ	9.95	9.24
ALA 21	O	11.76	10.74
*HIS 27	Nδ1	12.01	10.34
*HIS 27	Cδ2	12.41	8.25
*HIS 27	Cε1	19.28	9.67
*HIS 27	Nε2	20.27	9.90
TRP 59	Cδ1	5.23	4.27
TRP 59	Nε1	6.41	5.97
PRO 60	O	5.87	5.70
ILE 61	Cδ	7.77	4.81
LEU 62	Cγ	8.39	8.25
LEU 62	Cδ2	11.36	8.82
SER 64	Cβ	16.08	15.60
SER 64	Oγ	21.17	17.10
SER 64	O	18.10	17.82
GLY 65	O	16.78	15.17
VAL 67	Cβ	13.66	11.62
*VAL 67	Cγ1	18.64	11.01
*VAL 67	Cγ2	20.50	11.57
*TYR 68	Cε1	7.82	7.20
*TYR 68	Cε2	14.26	7.85
TYR 68	Cδ2	13.50	7.81
TYR 68	Cζ	9.27	9.12
SER 69	Oγ	18.94	18.77
PHE 80	Cε1	11.82	9.86
PHE 80	Cε2	10.31	7.80
PHE 80	Cζ	13.08	8.62
*HIS 92	Cε1	5.40	2.00
*HIS 92	Nε2	4.85	2.00

*Paired about a χ_1 or χ_2 axis.

TRP-59. In addition, we note that two atoms in the five-atom ring of TRP-59 are among those in which $B < 8\pi^2\langle x^2\rangle$ (Table 1). Together, these data suggest that the TRP-59 environment is even more dynamically restricted in the protein crystal than in our simulation.

II. Components of the anisotropy decay

The simulation trajectory was reoriented such that the average position of the TRP-59 rings is in the X-Y plane with the long axis of the residue aligned with the X axis. Angular fluctuations of the TRP rings with respect to these axes are shown in Fig. 2, *a–c*. It is readily seen that the angular rotations of the ring system are indeed isotropic in space and occur on a time scale on the order of

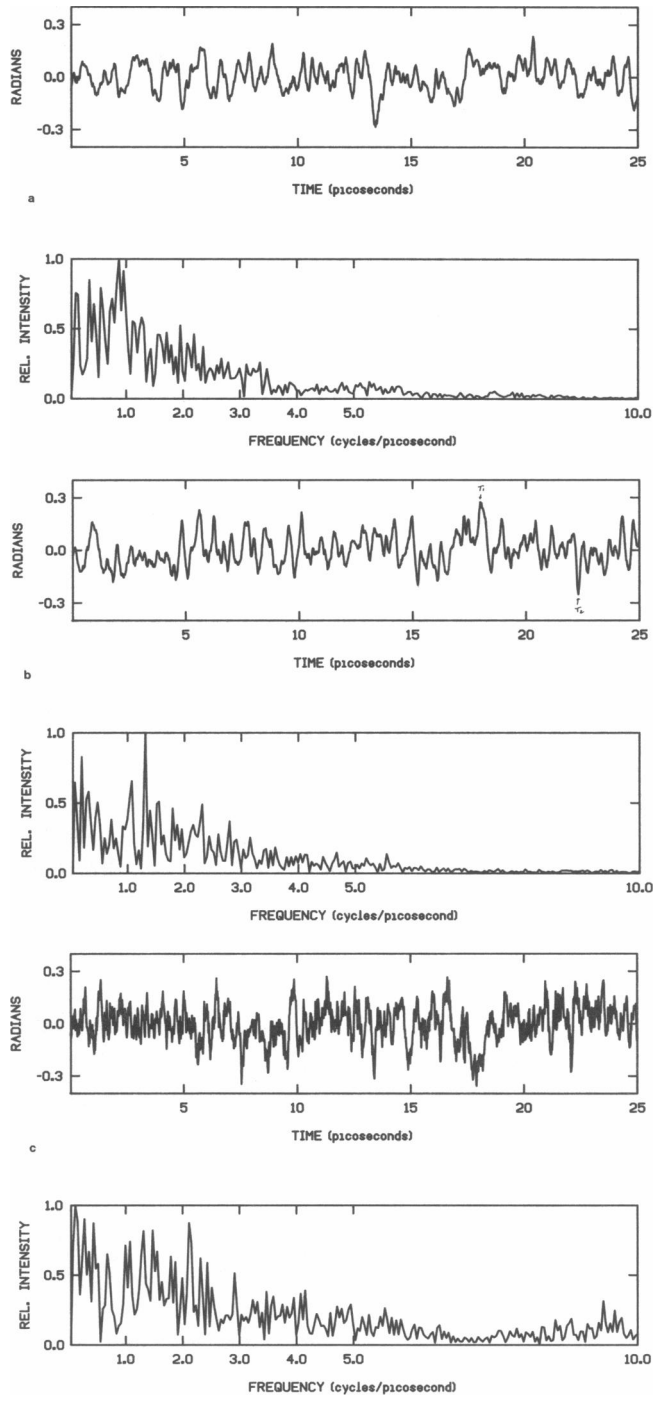

FIGURE 2 Fluctuation time series and their spectral densities for the last 25 ps of the simulation. The long axis is defined as the vector from the midpoint between atom $C_{\eta 2}$ and $C_{\zeta 3}$ to atom $C_{\delta 1}$. The short axis was defined as the vector from atom $C_{\delta 2}$ to $C_{\epsilon 2}$. Their cross product defines the perpendicular axis which in turn defines the plane of the rings. (*a*) In-plane fluctuations of the long axis; (*b*) out-of-plane fluctuations of the long axis, (times T_1 and T_2 correspond to Fig. 10; *a* and *b*). (*c*) Out-of-plane fluctuations of the short axis.

1 cycle/ps. There is little motion of the long axis faster than 5 cycles/ps but the short axis has significant motional components at 9–10 cycles/ps. The resolution of the data is 25 cycles/ps (sampling at 0.02-ps intervals).

Rotations about dihedral angles X_1 and X_2 are uncorrelated over time. The X_1 angle distribution mode occurs at ≈180 degrees and the energy of this torsion rarely exceeds 0.2 kcal/mol. In contrast, the X_2 angle distribution mode occurs at −110 degrees (the angle formed by $C_{\delta 1}$—C_γ—C_B—C_α) which corresponds to an eclipse of $H_{\delta 1}$ on C_β. Consequently, this torsion energy tends to be at a local maximum, ≈1.5 kcal/mol, and rarely is found below 1.0 kcal/mol. This energy barrier is too small, with barrier crossing being too frequent (≈2 cycles/ps), to be the basis for a two-state system yielding a double exponential fluorescence lifetime decay in RNAse-T1. Rather, for times greater than a few picoseconds these environmental influences on each conformer will be averaged.

III. VDW interactions

A. Search scheme

To find the most significant VDW interactions between TRP-59 and atoms of the protein matrix, a pair list was constructed between atoms of the TRP side chain (15 atoms) and all atoms whose average position over the course of the 50-ps trajectory was within 7 Å of any side chain atom (299 non-TRP protein and water atoms). For each of the 15 × 299 = 4,485 pairs, the maximum and mimimum VDW interaction energy was found over the duration of the trajectory and a maximum amplitude for the VDW energy fluctuation was calculated. The pair list was then sorted once to yield an ordered list of maximum interaction energies and again to yield an ordered list of maximum energy fluctuation amplitudes.

B. Descriptive summary

The pair-wise interaction energies ranged between −0.2 and +3.8 kcal/mol, and the instantaneous energies of the 25 pairs with the highest maximum interaction energies are shown plotted versus time in Fig. 3. In this figure, lines 1 and 3 show a persistent interaction between a water molecule and the five-member ring of TRP-59. Line 6 documents the appearance of a new water interaction with the six-member ring late in the trajectory. These interactions will be described in detail below in the section on solvent behavior.

Lines 2, 12, 15, and 23 suggest a slight relaxation of contacts involving these atoms over the course of the simulation, whereas the interactions represented by lines 4, 13, and 14 intensify slightly over the same interval. These data nonetheless reflect very small atomic displacements and, taken together with the remaining lines documenting stable interaction patterns, they indicate that atomic relationships in the immediate vicinity of TRP-59 are relatively stable during the simulation.

We note that RNAse-T1 was crystallized and crystallographically studied at a pH of 4.0–4.4 in alcohol solution with bound 2′-GMP (Heinemann and Saenger, 1982), whereas our simulation was conducted without ligand and with residues in their expected state of protonation at neutral pH. While the fluorescence intensity decay of TRP-59 in RNAse-T1 at acid pH appears to be purely monoexponential, a short component (τ = 1.0–1.5 ns) is present at neutral pH (Chen et al., 1987; Eftink and Ghiron, 1987). In addition, new intensity decay components are observed upon the binding of ligand to a site which is not in direct contact with the fluorophore (Chen et al., 1987; MacKerrel et al., 1987). It seems reasonable to infer from these data that pH manipulations and ligand binding both induce conformational shifts in the protein.

Therefore, insofar as the initial structure for our simulation was that of the "liganded acid pH" form, the "unliganded neutral pH" form should evolve in the course of the trajectory, representing a mixture of ligand- and pH-induced conformational shifts. The increasing or decreasing interaction intensities mentioned above may in fact be manifestations of such an evolution.

The TRP-59 side chain interactions in Fig. 3 are strictly nonpolar with the exception of lines 12, 14, 15, and 23 which document contacts between various side chain atoms and the carbonyl oxygens of ALA-19, TYR-38, and PRO-60. In total, we observe 152 separate repulsive VDW contacts between TRP-protein atom pairs in the course of the simulation; 20 of these pairs may be seen to involve TRP and polar atoms (see Table 2). This list illustrates the utility of a dynamics simulation in this type of analysis, because interactions of this type could not be easily or reliably generated from the crystal structure of energy-minimized coordinates. These data suggest that most atoms in the TRP-59 side chain frequently collide with polar atoms (at least once in 50 ps). This is an unexpected finding because, by spectroscopic criteria, TRP-59 appears to be in a relatively nonpolar environment (James et al., 1985).

C. Proline-39

Several intriguing interactions involve atoms of a *cis*-proline at position 39 and the six-atom ring of TRP-59 between 15 and 16 ps into the simulation (lines 7, 10, 11, 16, and 18). Inspection of the trajectory at this point shows PRO-39 to undergo a conformational transition characterized by boat-chair (axial-equatorial) shifts of the ring C-H bonds (Fig. 4 and Table 3). In the "boat" form, both the carbonyl group and atom C_γ are found on the same side of the plane formed by atoms C_δ—N—C_α, whereas these atoms are on opposite sides of this plane in the "chair" form.

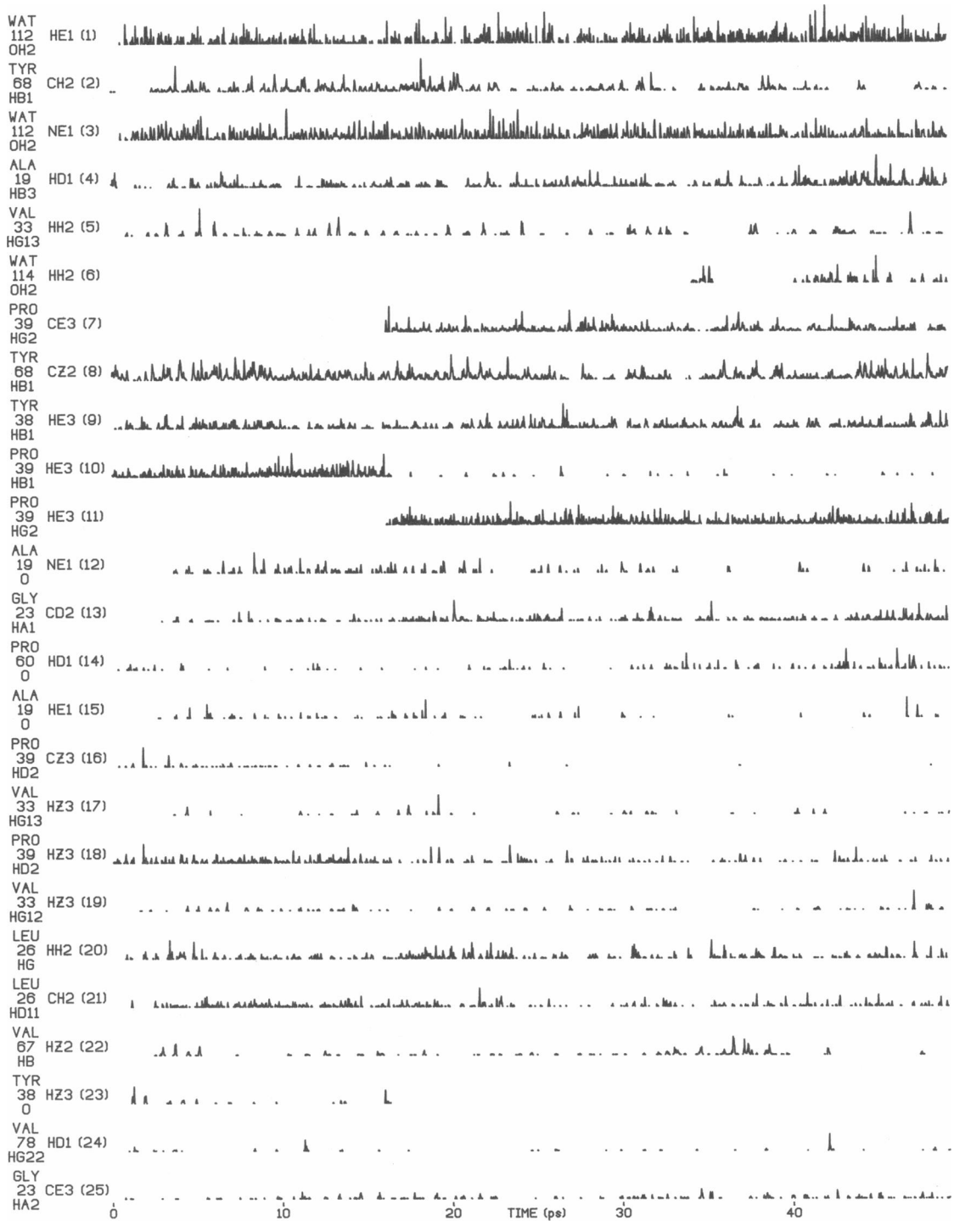

FIGURE 3 VDW interactions between TRP-59 atoms and other atoms in the protein matrix or solvent. Complete (50 ps) time series for the 25 largest interactions are shown. The largest energy of interaction is 3.8 kcal/mol and all plots are on the same scale. The energy is not plotted when it is less than zero.

TABLE 2 VDW interaction energies ("contacts") between atoms of TRP-59 and polar atoms of the protein and solvent

Max (*E*)	TRP-atom	PROT-atom	Max (*E*)	TRP-atom	WAT-atom
0.084	Nε1	ALA C 19	0.308	Cη2	O 114
0.749	Hδ1	ALA C 19	0.071	Hη2	H 114 1
0.880	Cδ1	ALA O 19	0.029	Hη2	H 114 2
1.263	Hδ1	ALA O 19	2.704	Hη2	O 114
2.043	Hε1	ALA O 19	0.054	Hζ3	O 114
2.149	Nε1	ALA O 19			
0.002	Cε2	GLY N 23	0.234	Hη2	H 227 1
0.391	Hζ3	TYR C 38	1.359	Hη2	O 227
1.761	Hζ3	TYR O 38	0.823	Hζ2	O 227
0.072	Hε3	PRO N 39			
0.165	Hζ3	PRO N 39	0.161	Hη2	O 228
0.012	Hδ1	TRP C 59			
0.168	Cδ1	TRP C 59	0.408	Hη2	O 354
1.534	Cγ	TRP C 59	0.648	Hζ2	O 354
0.230	Hδ1	PRO C 60			
0.629	Nε1	PRO O 60	0.016	Cδ1	O 112
1.208	Cδ1	PRO O 60	0.006	Cδ1	H 112 2
2.052	Hδ1	PRO O 60	0.168	Cε2	H 112 1
0.066	Hζ2	TYR N 68	0.524	Cε2	O 112
0.206	Hζ2	TYR HN 68	0.886	Cζ2	O 112
			1.197	Hζ2	O 112
			1.178	Nε1	H 112 1
			0.478	Nε1	H 112 2
			3.153	Nε1	O 112
			3.793	Hε1	O 112

All interactions with an energy greater than zero have been included. Values were calculated using the VDW term of the CHARMM potential function and VDW parameters from Brooks et al. (1983).

A separate 500-ps vacuum simulation of the isolated proline zwitterion at 300°K revealed that the preferred conformer in the CHARMM potential field is the chair form, but a single spontaneous transition to the boat form was observed along with many occurrences of a planar configuration. The single occurrence of the boat form lasted ≈1.0 ps.

In addition, an adiabatic mapping of this transition was done using the 14 atoms present in PRO-39 and fixing the positions of atoms N, C, and O to their relative positions in the RNAse-T1 crystal. The dihedral angle defined by atoms C_γ—C_δ—C_β—C_α was constrained at intervals of 2.5 degrees through a range of −75 to +75 degrees and exhaustively energy minimized at each step. This mapping reveals an energy minimum at −42.5 degrees corresponding to the chair form, and at 45 degrees corresponding to the boat form, with the chair form more stable by 1.55 kcal/mol. The difference is due chiefly to a reduced repulsive electrostatic term in the chair form between the carbonyl oxygen (assigned charge = −0.55) and atom C_γ (assigned charge = −0.2). The barrier for interconversion was 4.6 kcal/mol above the internal energy of the chair form.

Whether these energy differences correspond to a true conformational preference is unknown. Tanaka et al. (1977) have reviewed crystal studies of pyrrolidine ring conformations in short peptides, noting that both forms are found. A brief survey of the better resolved structures in the Brookhaven Protein Data Bank also finds both forms represented (data not shown). However, protein crystal structures are difficult to interpret on this scale due to their relatively low resolution; conformers found in such data most likely represent the bias of the refinement procedure rather than actual conformational detail.

Nonetheless, given the CHARMM potential function and the available crystal data, PRO-39 is initially in an energetically unfavorable conformation, and a transition to the favored conformation occurs after 16.0 ps in our simulation. This transition could be related to the evolution from a liganded-acid-pH form to an unliganded-neutral-pH form of the enzyme as mentioned above. This is especially plausible because PRO-39 is adjacent to a histidine residue at position 40. The finding that the transition does not occur earlier, as would be expected recalling the brief existence of this conformer in the vacuum simulation, suggests either that adjacent atoms sterically interfere with the transition, or various nonbonded interactions in the protein crystal tend to stabilize the boat form.

IV. Solvent behavior

A. Structural water

A single water molecule (designated WAT-112) lies near the surface of the protein in a small cavity for the entire simulation. This cavity is not accessible to a 1.4 Å probe sphere from the protein exterior and the water within it is apparently stabilized by hydrogen bonds. The presence of this water was predicted by the simulation and subsequently confirmed by the x-ray crystallographic data (Arni et al., 1987). Fig. 5 illustrates the relationship between potential H-bond pairs in the vicinity of TRP-59 and shows that an H-bond chain may extend from WAT-112 out to bulk water via WAT-142 and WAT-110. The distribution of geometric relationships between the oxygen of WAT-112 and $H_{\epsilon 1}$ of TRP-59 are shown in Fig. 6 *a*.

Our simulation considered electrostatic energies involving polar hydrogens but did not explicitly consider H-bond energies by the incorporation of directional terms

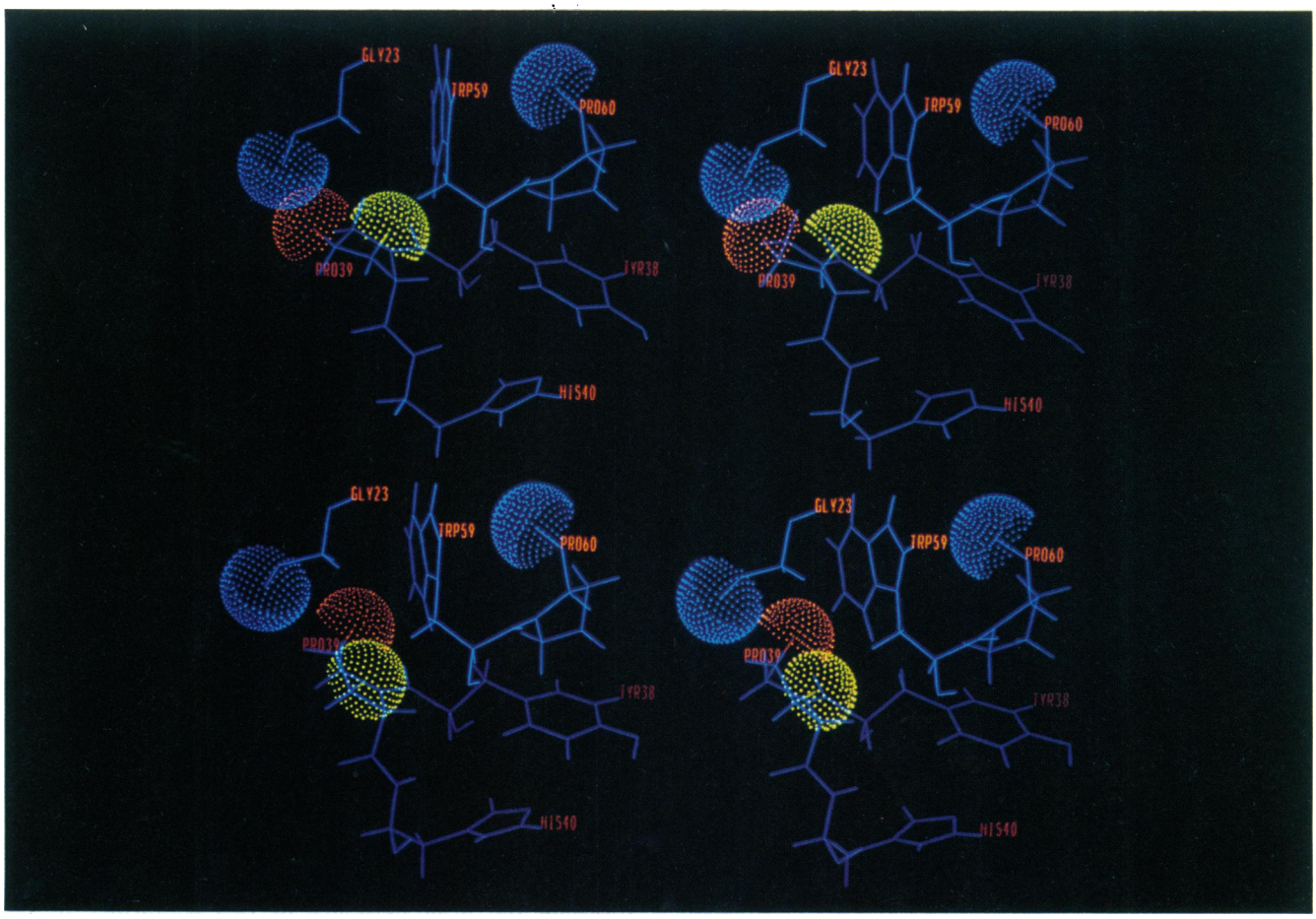

FIGURE 4 The relationship between PRO-39 and TRP-59 before (above) and after (below) the transition at 16 ps. Connolly surfaces have been placed on the carbonyl oxygens of residues GLY-23 and PRO-60 (shown in blue) and PRO-39 atoms $H_{\beta 1}$ (yellow) and $H_{\gamma 2}$ (red). It appears that part of the PRO-39 ring is held away from the TRP-59 rings by the GLY-23 carbonyl. After the transition, the PRO-39 ring is free to collide with a face of the TRP-59 and possibly displace TRP-59 in the direction of the PRO-60 carbonyl.

(e.g., a term representing quadrupole moments for peptide N–H groups) into the potential function. Hence, H-bond energies must be estimated from the observed geometries, and it may be expected that incorporation of a directional term into the potential function would change the distribution of these geometries. Nevertheless, it is evident from Fig. 6 *a* that the geometries are favorable for H-bond formation as well as significant electrostatic interactions between the indole >N—H group of TRP-59 and WAT-112. In addition, significant interactions seem likely involving the carbonyl groups of PRO-60 and ALA-19 as well as the peptide hydrogen of TYR-68. Geometry distributions for these pairs were much less favorable for H-bond formation, however (Fig. 6, *b* and *c*).

TABLE 3 Characteristics of PRO-39 before and after a transition occurring at 16 ps

Time relative to transition	Before		After	
Conformer	Boat		Chair	
Interacting pairs	TRP-Cζ3	PRO-Hδ2	TRP-Hε3	PRO-Hγ2
	Hζ3	Hδ2	Cε3	Hγ2
	Hε3	Hβ1		

B. Solvent water

In addition to the above-mentioned structural water, another 203 water molecules were explicitly modeled within the 16 Å boundary. In simulations consisting of only water within such a boundary, we have noted that there exists a region of above-average density located in a shell just inside the boundary. It is difficult to calculate water density in our simulation of RNAse-T1 because there are few regions inside the boundary >4 Å from

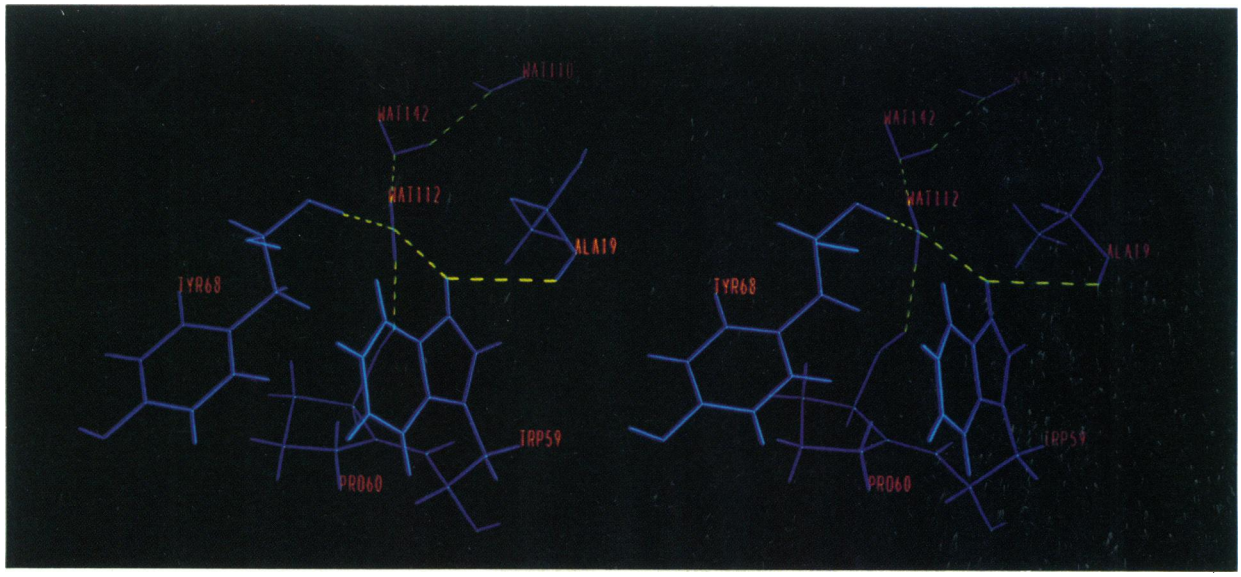

FIGURE 5 Electrostatic interactions involving the indole >N—H group of TRP-59 and WAT-112. Data represent crystal coordinates with hydrogens positioned in an energy-minimized configuration by CHARMM. Residues ALA-19, TRP-59, PRO-60, TYR-68, WAT-112, WAT-142, and WAT-110 are shown along with potential (not necessarily actual) hydrogen bonds.

protein and therefore not dominated by the presence of the protein. Nevertheless, in such regions as there are, the water appears to recede slightly from the boundary and condense toward the surface of the protein.

Given that initial solvent positions were assigned quite arbitrarily, an equilibration period must pass before the simulation can be expected to exhibit realistic relationships between protein and solvent. The requisite length of such a period is unknown, but it is clear that migration of the water toward the protein surface is generally complete

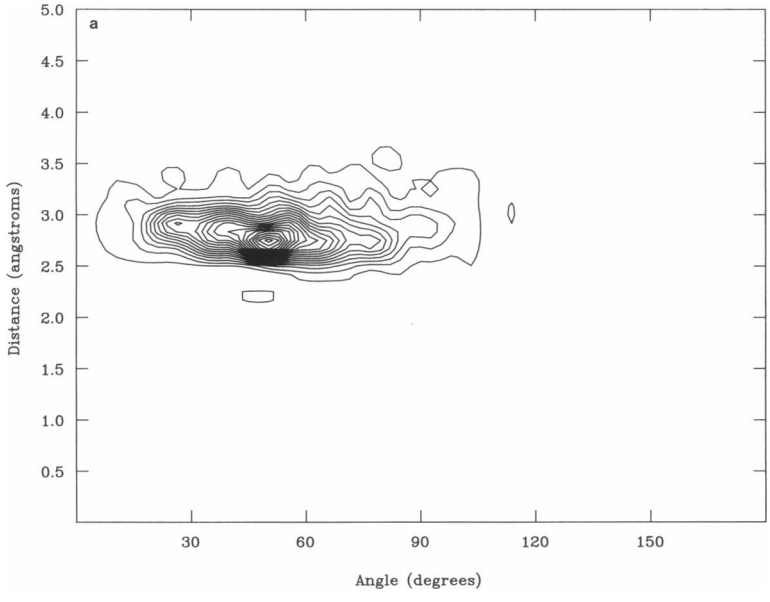

FIGURE 6 Distribution of hydrogen bond geometries involving TRP-59. The D-A distance and D-H-A angle for the indicated atoms were calculated for each of the 1,250 data sets comprising the last 25 ps of the simulation and plotted to show the distribution of geometries and angles. D, donor, H, hydrogen, and A, acceptor. Contour levels are arbitrary. (*a*) $H_{\epsilon 1}$ (TRP-59) and the oxygen of WAT-112. (*b*) $H_{\epsilon 1}$ (TRP-59) and the carbonyl of ALA-19. (*c*) $H_{\epsilon 1}$ (TRP-59) and the carbonyl of PRO-60.

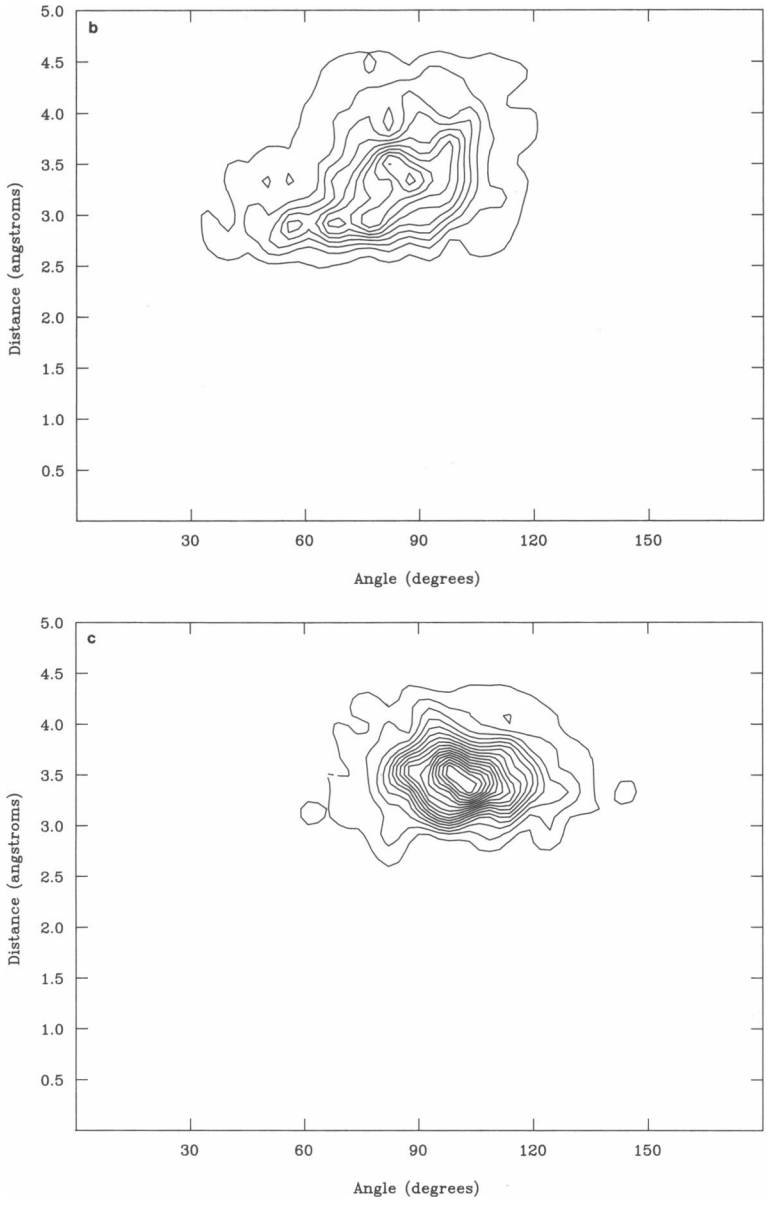

FIGURE 6 continued

by 20 ps. The time series presented below should be considered in this light, even though they are depicted for the entire simulation length of 50 ps.

We have examined the interaction between water and TRP-59 as a model for the interaction of quenching agents and this residue, particularly quenching agents with hydrogen bonding capability such as acrylamide or trichloroethanol. In the course of the simulation, 21 contact pairs are observed (see Table 2). Of note, the most energetic of these contacts involve the water oxygen; water hydrogen contacts are relatively weak. The most intense interactions occur between the oxygen of WAT-114 and atom $H_{\eta 2}$ of TRP-59, and it is of interest to correlate these interactions with the solvent-accessible surface area of the TRP residue (see Fig 7).

Several features of Fig. 7 are noteworthy. First, the accessible surface area (algorithm of Lee and Richards, 1971) fluctuates rapidly, rarely being equal to zero and occasionally as high as 5 Å. Atom $H_{\eta 2}$ accounts for 93% of this area. In the free amino acid form of TRP, this atom has a total accessible surface of 35 $Å^2$ whereas the indole moiety apart from the protein backbone has a surface

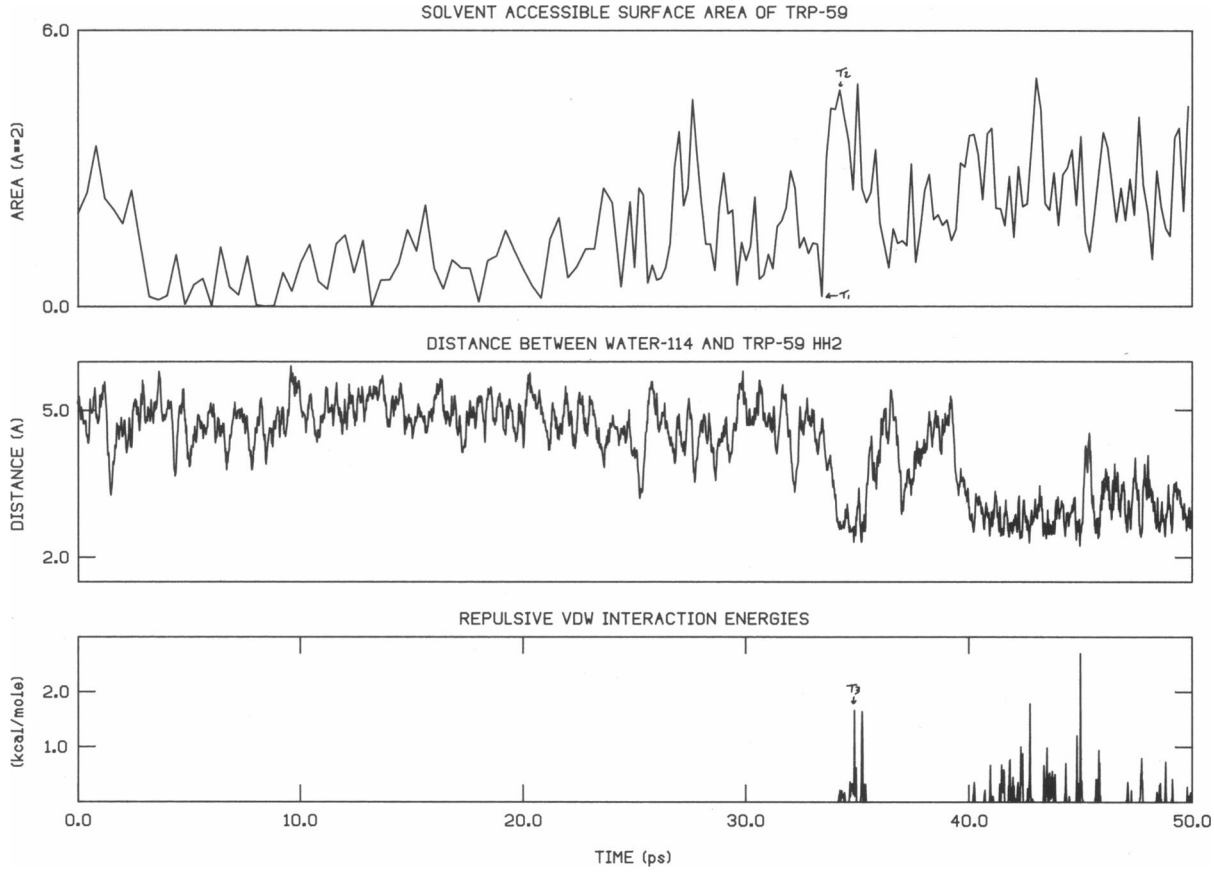

FIGURE 7 The interaction of WAT-114 and TRP-59. (*a*) The solvent-accessible surface was calculated at 0.2-ps intervals throughout the 50-ps simulation using the algorithm of Lee and Richards (1971). The initial value was 2.0 Å^2 (*b*) The distance between the oxygen of WAT-114 and atom $H_{\eta 2}$ of TRP-59. (*c*) Positive VDW interaction energies between the oxygen of WAT-114 and atom $H_{\eta 2}$ of TRP-59. This is the same plot as line 6 of Fig. 3. Times T_1, T_2, and T_3 correspond to Fig. 8 *a*, *b*/*c*, and *d*.

area of 230 Å^2. By the same measure, RNAse-T1 has a total surface area of 4,000 Å^2. Second, although an apparent equilibration process takes place in the first 40 ps of the trajectory, the average area in the last 10 ps (~2.5 Å^2) is the same as that found for the crystal structure (see ordinate at time = 0.0 ps). Third, it is seen that WAT-114 is in close proximity (≈5 Å)to atom $H_{\eta 2}$ throughout the trejectory, but only makes repulsive contact at later times. These latter two features may in fact indicate that this water assumes an "equilibrated" position only at these later times.

Analysis of the trajectory using computer graphics clarifies certain features of these data (Fig 8). WAT-114 appears to preferentially participate in a hydrogen bond network with polar moieties on the protein surface and with other waters. These interactions suspend WAT-114 somewhat above TRP-59 for most of the simulation, leaving an unoccupied space adjacent to TRP-59 with a volume less than that of an oxygen atom. The solvent-accessible surface of TRP-59 (algorithm of Connolly, 1983) forms the base of a shallow pit on the protein surface which is almost completely bounded by nonpolar atoms. There is an apparent competition for H-bonding partners between WAT-114 and the nearby peptide hydrogen of TYR-68; WAT-114 occupies the space adjacent to TRP-59 only when the water to which it is H-bonded has instead H-bonded to TYR-68. Contact between WAT-114 and $H_{\eta 2}$ is further facilitated by the concerted movement of TRP-59 toward the protein surface and rotation of adjacent residue side chains such that the "window" to $H_{\eta 2}$ is slightly larger.

V. Electrostatic interactions

A. General considerations

We have considered three ways of examining the electrostatic environment of the TRP side chain in RNAse-T1. The first merely lists which atoms interact most strongly

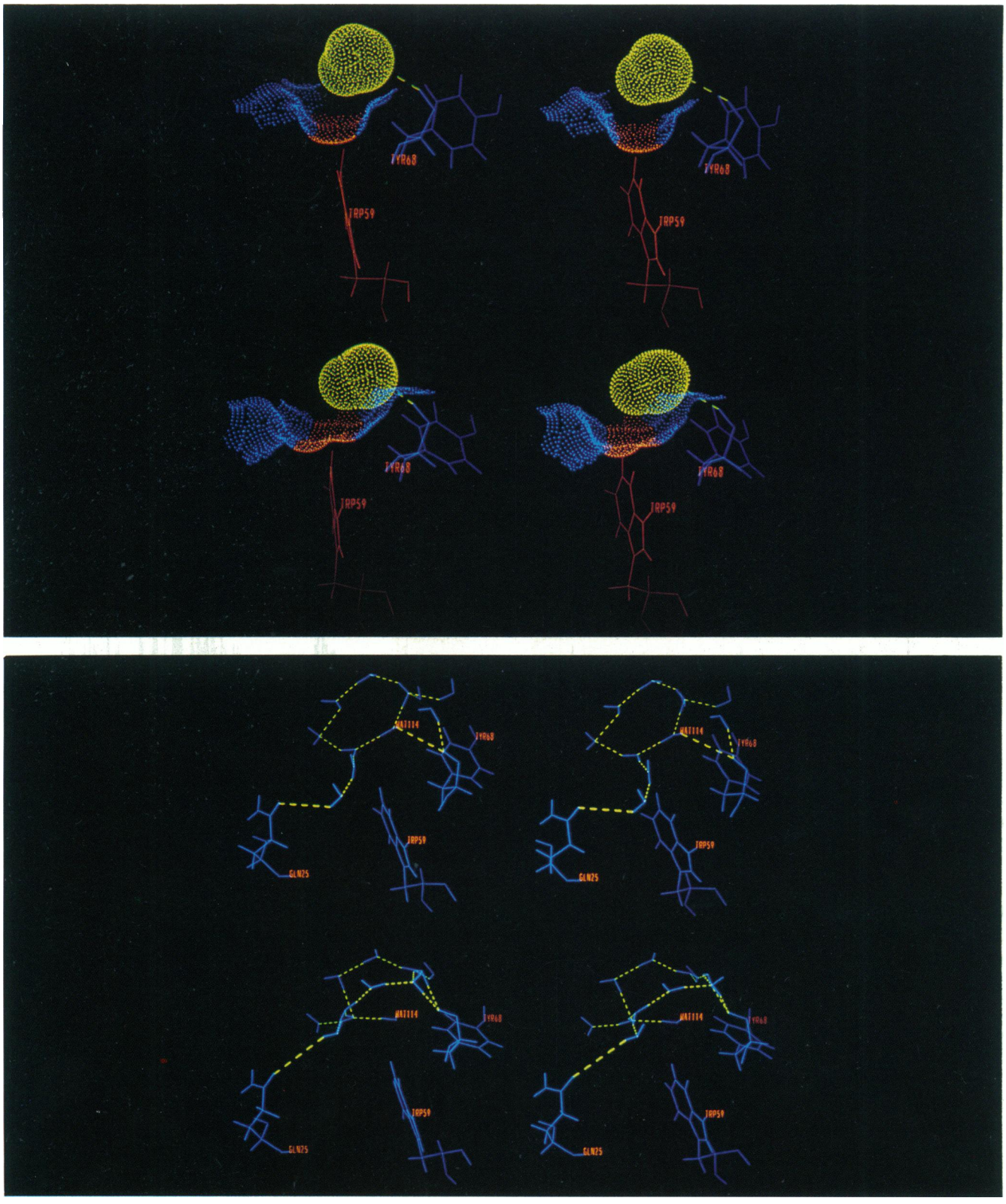

FIGURE 8 Interactions of WAT-114 and TRP-59. A solvent-accessible (Connolly) surface has been placed on RNAse-T1 at points corresponding to times T_1 and T_2 in Fig. 7. Red: TRP-59. Yellow: WAT-114. Blue: other protein atoms. (*a*) Time 33.42 ps: TRP-59 is minimally "accessible" at this point and WAT-114 is suspended above the TRP-59 surface by hydrogen bonds to TYR-68 and other waters. (*b*) Time 33.84 ps: TRP-59 has transiently moved toward the surface and adjacent residues (particularly GLN-25 and TYR-68) have rotated such that TRP-59 is far more accessible to solvent. The Lee and Richards surface area algorithm (used in Fig. 7) indicates a 25-fold increase in solvent accessibility over this interval. If we had distinguished between contact and reentrant Connolly surfaces in this figure, a correspondingly large increase in the contact area would be evident. (*c*) Time 33.84 ps (same as *b*): WAT-114 participates in a hydrogen bond network with other waters and polar protein groups such as the GLN-25 side chain and the TYR-68 main chain. Although TRP-59 is "accessible," there is no VDW contact at this point. (*d*) Time 34.20 ps: WAT-114 makes contact with TRP-59 only after breaking hydrogen bonds with TYR-68 and another water molecule (time T_3 in Fig. 7).

with atoms of the TRP-59 side chain. The second considers which of these interactions fluctuate over the broadest range. The former constitute the principal electrostatic influences on the TRP-59 side chain, whereas the latter reveal time-dependent interactions which may significantly though transiently change the electrostatic field of the side chain. The third approach involves constructing a molecular electrostatic potential map in the plane of the TRP side chain. The application of macromolecular mechanics to the analysis of protein electrostatics sidesteps most quantum mechanical considerations including the fact that one must work with energy and time scales that are well beyond the Heisenberg uncertainty threshold. Each of these approaches, though based on the potential used in calculation of the trejectories, must be regarded as no more than semiquantitative because it is not possible at this stage of the work to consider atomic polarizabilities and quantum mechanical effects rigorously. A simplistic electrostatic treatment notwithstanding, this approach to molecular dynamics has demonstrated noteworthy experimental correlations. For example, molecular dynamics estimates of the energy barrier height for tyrosine ring rotation (Ghosh and McCammon, 1987), of ligand-receptor binding energies (Bash et al., 1987), and of fluorescence anisotropy decay (Axelsen et al., 1988) all correlate to experimental data with reasonable accuracy.

B. Search scheme

The most significant electrostatic interactions were found in parallel with the search for VDW interactions described above. A constant, unshifted dielectric of 1.0 and the partial atom charges assigned by CHARMM were used. No polarization or shielding effects were assumed, and only monopole–monopole energies were calculated using: $E = q_1q_2/(4\pi\epsilon r)$, where r is the interatomic distance and ϵ is the permittivity of the vacuum. Charges assigned to TRP ring atoms by CHARMM are given in Table 4. Minimum and maximum interaction energies (absolute values) were found as for VDW interactions above for each of the 4,485 atom pairs studied at each time point over the course of the simulation. Ordered lists of the maximum energy and maximum energy fluctuation amplitude were prepared.

C. Descriptive summary

Ordered lists of peak interaction energies and interaction energy fluctuations were very similar, indicating by one measure that specific electrostatic interactions with relatively high energies are not preferentially observed in the simulation. Time series of these energies reveal some trends involving TRP-water pairs that may be due to an equilibration process, but no such trends among TRP-protein pairs are observed beyond the first 3 ps (see Fig. 9). As expected from the partial charge assignments (Table 4), the most energetic interactions involve the indole >N—H group of TRP-59. Interactions with a structural water (WAT-112) predominate, and involve an apparent H-bond (see above discussion of "structural water").

TABLE 4 Partial atom charges assigned to TRP sidechain atoms by CHARMM and used in electrostatic energy calculations

5-Atom ring		Inter-ring		6-Atom ring	
Cγ	−0.03	Cδ2	0.10	Cε3	−0.13
				Hε3	0.10
Cδ1	−0.04	Cε2	−0.04		
Hδ1	0.10			Cζ2	−0.10
				Hζ2	0.10
Nε1	−0.36				
Hε1	0.30			Cζ3	−0.10
				Hζ3	0.10
				Cη2	−0.10
				Hη2	0.10

Sum of the charges is zero.

There are relatively large interaction energies with the carbonyl groups of both ALA-19 and PRO-60, the former being larger, generally. These interactions begin to occur intermittently 3 ps into the trajectory and frequently return to the relatively low level found in the crystal structure throughout the trajectory. This suggests that both relatively high energy and relatively low energy interactions with the ALA-19 carbonyl occur, and the neither is merely an artifact of incomplete equilibration. The geometry of this $H_{\eta 1}$-carbonyl interaction does not appear likely to yield true H-bonds of significant energy (see Fig. 6 *b*), however, we do not know the extent to which use of explicit H-bond terms in the CHARMM potential function would alter the distribution of observed geometries.

Several other water molecules develop relatively large interaction energies with the indole >N—H group, but are in continuity with bulk water rather than individually situated in the protein matrix as with WAT-112. Excluding water and the >N—H group, electrostatic interaction energies between protein matrix and the TRP-59 side chain are relatively low in energy (<8 kcal/mol), and stable over the course of the trajectory. This set of interactions involves predominantly backbone carbonyl groups interacting with both TRP rings. These carbonyl groups (bearing partial charges of +0.55/−0.55) are generally found to be oriented with the oxygen closer to the TRP rings. Backbone N—H groups are assigned smaller partial charges (+0.25/−0.35) and consequently, the only N—H group found in a list of the 100 strongest interactions is that of TYR-68; in this case the

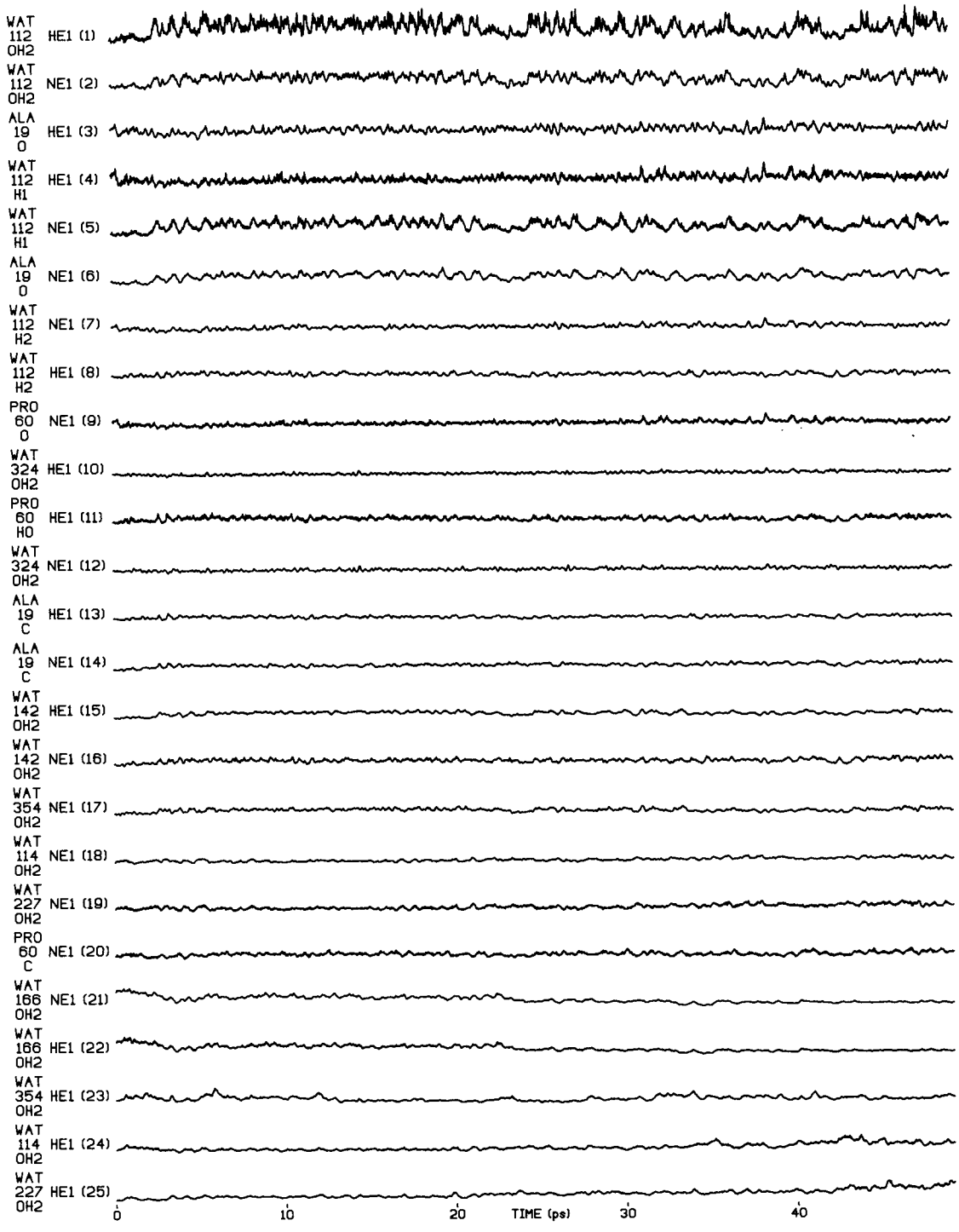

FIGURE 9 Electrostatic interaction energies between TRP-59 atoms and other atoms in the protein matrix or solvent. Complete (50 ps) time series for the 25 largest interactions are shown. For reference, the range of energies in line 1 is 22.3–48.5 kcal/mol and all plots are on the same scale.

peptide hydrogen is oriented toward atom $H_{\zeta 2}$ of TRP-59.

D. Molecular electrostatic potentials

Electrostatic potential maps were constructed at various points in the simulation by determining the sum of the potentials due to all protein and water charges for a grid of points in the plane of the TRP side chain. As with the above calculations, no polarization or shielding effects were assumed, and the potential at each point was calculated using $V = \Sigma_{i=1}^{n} q_i/(4\pi\epsilon r)$ over the n atoms for which distance $r < 8$ Å from the grid point (exclusive of TRP side chain atoms). The resulting maps resemble published molecular electrostatic potentials for small molecules calculated using semempirical and *ab initio* programs (Politzer and Truhlar, 1981). However, it is not presently feasible to apply these more rigorous programs to structures as large as proteins. It is possible to refine this calculation somewhat by the introduction of terms accounting for atomic polarizabilities (Russel and Warshel, 1985); however, uncertainties with respect to partial charge parameters may not warrant such refinement (Van Belle et al., 1987). Hence, for the present, our relatively crude and semiquantitative maps must suffice.

The most noteworthy result from these studies is that the potential maps for two extremes of TRP-59 side chain rotational motion are remarkably similar (see Fig. 10, *a* and *b*). Thus, by this measure, and despite the specific electrostatic energy fluctuations noted above, the environment of TRP-59 in RNAse-T1 appears electrostatically homogeneous throughout the rotational excursion of the side chain. We also find that TRP-59 is situated near the midpoint of the helix where the helix macrodipole will have relatively weak interactions with TRP-59 regardless of orientation. Finally, we note that unbound water tends to oppose whatever small gradient is due to the helix.

To put these results into perspective, we have compared them to maps made from the crystal structures of azurin and staphylococcal nuclease (see Fig. 10, *c* and *d*). In azurin, we see that the potential is smaller in magnitude, but that the gradient in the plane of the rings is severalfold greater at most points. In nuclease, the potential is highly positive as well as more steeply graded. Thus, we conclude that the electrostatic environment of TRP-59 in RNAse-T1 is relatively homogeneous, and that substantially greater potential gradients may act on the TRP side chain in other proteins.

DISCUSSION

I. Analytical validity

The accuracy of a molecular dynamics simulation is very difficult to assess when the object of study is a single macromolecule. In single-TRP proteins, a simulation of fluorescence anisotropy decay can be compared with the experimentally determined limiting anisotropy. However, a comparison such as this is only capable of showing a simulation to be unrealistic, and it says little about a simulation which compares favorably. Apart from this, we must rely largely on self consistency within the simulation to assess its validity.

For example, to illustrate various approaches to the question of when a system is suitably equilibrated, we have included time series which span the entire 50-ps trajectory in most figures. Time series of electrostatic interactions appear to be largely insensitive to equilibratory processes because they begin a monotonous pattern within several picoseconds of simulation. Likewise, most of the VDW interactions reveal little change in character over 50 ps. On the other hand, the solvent-accessible TRP surface is clearly in transition over the same interval. We conclude that interactions such as that of TRP-59 with WAT-112 and the ALA-19 carbonyl group are consistently represented throughout most of the simulation, whereas the solvent accessibility of TRP may or may not be suitably represented by the end of the trajectory. Singular events such as the PRO-39 conversion at 16 ps are found fortuitously and even missed if an "equilibration" period is not given the same scrutiny as the "equilibrated" period.

There are at least two serious limitations encountered when specifically attempting to interpret fluorescence using the molecular dynamics approach. First, the time scale of the simulation is many orders of magnitude shorter than the time scale of the experiment. Thus, we sample only a minute portion of the conformational space available to a protein in a 50-ps simulation. Furthermore, even 100-fold longer times (times comparable to the fluorescence lifetime) are inadequate because evidence suggesting that the fluorophore environment in RNAse-T1 is heterogenous implicitly requires simulations many times longer than the fluorescence lifetime.

Second, the model for tryptophan used in molecular dynamics is, at best, a crude model of the ground state fluorophore. No adjustments are made for changes in kinetic energy or charge distribution incurred as a result of photoexcitation, nor is it clear how to make such adjustments. We might expect quantum mechanical calculations to yield insight into this problem, but here too, no adequate theory exists describing relaxation from the electronically excited singlet state. Furthermore, indole exhibits particularly complex photophysics with two closely spaced excited states, one of which is manifest only in condensed phases (Rizzo et al., 1986; Hager et al., 1987).

These limitations dictate that we must carefully avoid overinterpreting molecular dynamics simulations. In our

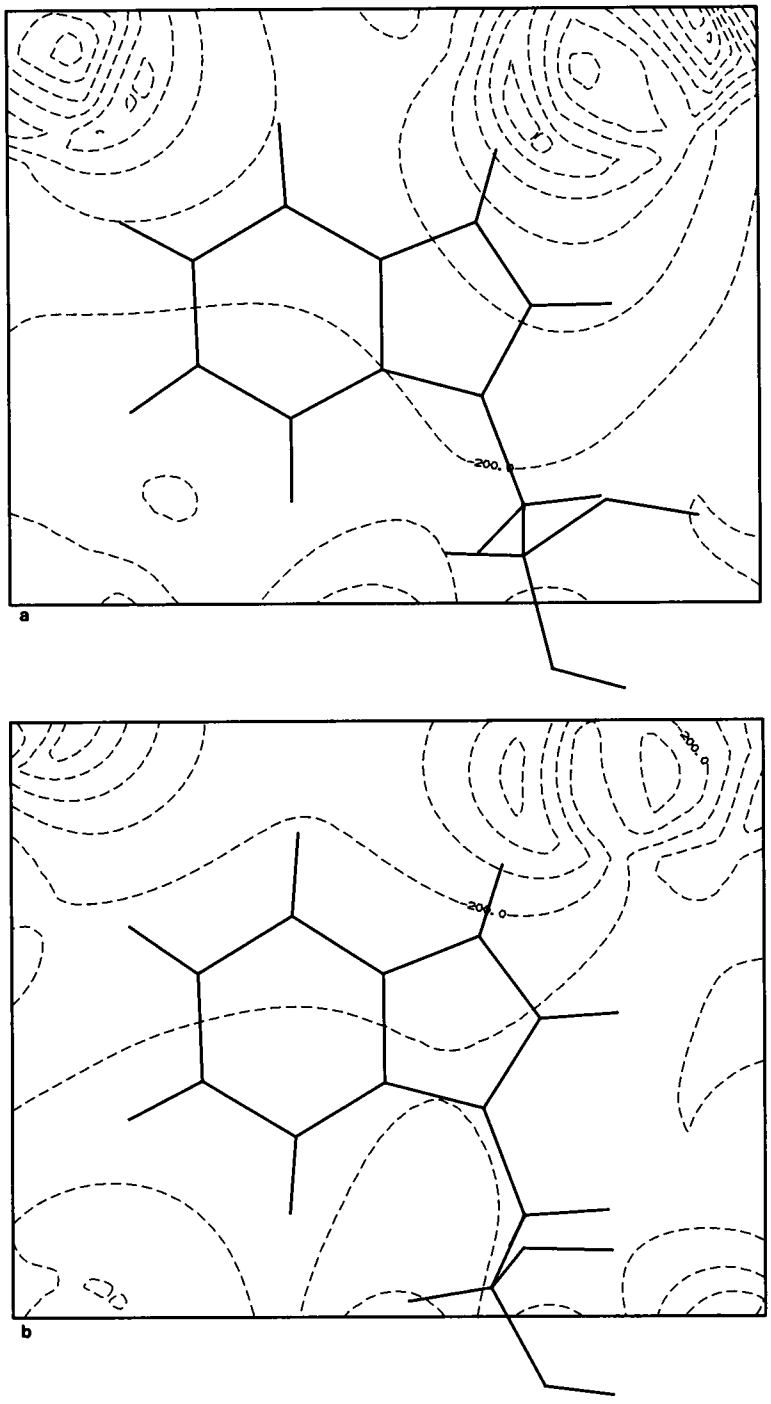

FIGURE 10 Molecular electrostatic potential maps. The electrostatic potential in the plane of the TRP rings is shown for two points in the simulation which represent the extremes of rotational motion for the TRP-59 side chain. (*a*) Map at 43.00 ps into the simulation (time T_1 in Fig. 2 *b*) (*b*) Map at 47.32 ps into the simulation (time T_2 in Fig. 2 *b*) Rings in panels *a* and *b* are oriented ~34 degrees to each other. (*c*) Map of azurin using crystal coordinates. (*d*) Map of nuclease using crystal coordinates. Note: Maps *a* and *b* include solvent water, whereas maps *c* and *d* do not. Dashed lines represent negative potentials; solid lines represent positive potentials; contour intervals of 10 kcal/mol per esu.

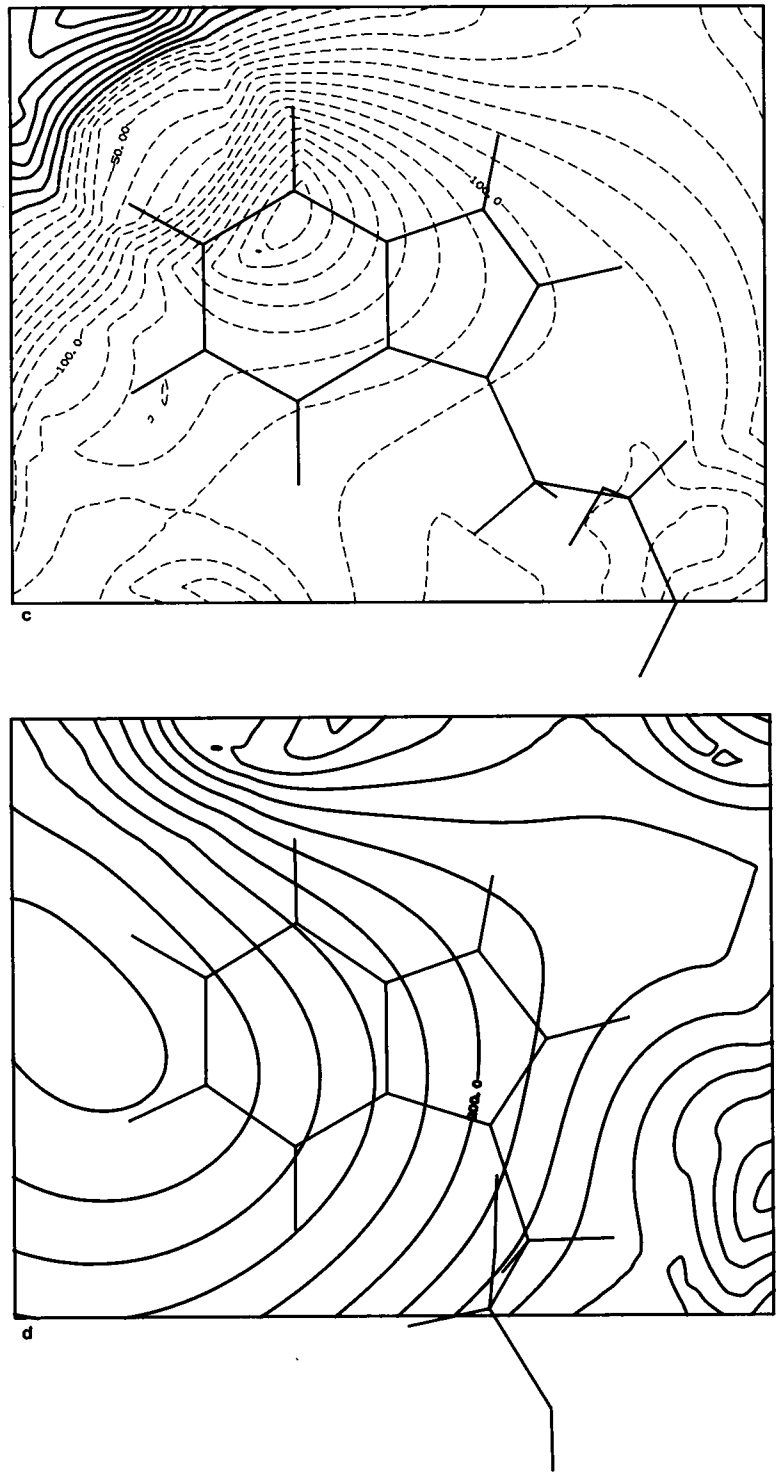

FIGURE 10 continued

view, we can best regard such brief simulations as a tool for a more detailed analysis of protein crystal structures. Through such analyses, we seek to gain insight into important aspects of the structure which are not ordinarily apparent in crystallographic data such as anisotropic motions and protein-solvent interactions. We also seek to avoid inappropriately rigid preconceptions concerning intramolecular interactions.

II. Anisotropy decay

The unoccupied space around TRP-59 apparent in the x-ray crystal structure of RNAse-T1 allows the side chain to rotate no more than ±5 degrees. The simulation, on the other hand, reveals frequent excursions to ±17 degrees. These excursions occur to an equal degree along all axes (Fig. 2, *a–c*) and reflect substantial motion of the protein matrix in the vicinity of TRP-59.

Assuming a limiting anisotropy, r_0, for TRP of 0.310, the simulated anisotropy decay for RNAse-T1 plateaus at a value of ≈0.298, which agrees well with published data (Lakowicz et al., 1983; Eftink, 1983; Axelsen et al., 1988). Although this corresponds to a 9.4-degree "cone of rotation," such abstractions do not relate in any simple way to the fact that we also observe rotational fluctuations as large as ±17 degrees (Lakowicz, 1983). For example, it is not correct to assert that "(a simulated anisotropy) decrease corresponds to an increase in the angle λ between the absorption and emission vectors", as stated by MacKerrel et al. (1987). These authors found an anisotropy decay from 0.31 to 0.24 in a vacuum simulation of RNAse-T1 for which the correct cone angle is 22.8 degrees. This is not consistent with experimental results showing smaller angles for TRP residues in most other proteins and an angle of ≈0 degrees in RNAse-T1 (Lakowicz et al., 1983; Eftink, 1983).

TRP side chain fluctuations must undoubtedly occur with an amplitude greater than the value of their cone angle, but we do not at present have any means to determine whether they occur to the extent or with the frequencies suggested by the simulation. Our results would be strengthened by demonstrating good correlations with experiment when comparable simulation strategies are applied to a series of single-TRP proteins exhibiting a range of limiting anisotropies.

Frequency-domain fluorescence spectroscopy promises to be an important technique for comparison of experiment to simulation with its capability of resolving anisotropy decays on the picosecond time scale (Lakowicz et al., 1986, 1987). For example, in RNAse-T1 there is no evidence for correlation times shorter than the overall correlation time for the protein (6.5 ns) using this technique, even with the use of acrylamide quenching (Lakowicz, J. R., unpublished results). Thus, the 100-ps correlation times measured by MacKerrel et al. (1987) and the 22-, 39-, and 130-ps times found in various simulations of RNAse-T1 (MacKerrel et al., 1987, 1988) may be high-temperature phenomena (40°C) or artifact.

III. Emission spectra

The fluorescence emission from TRP-59 in RNAse-T1 is unusual both for the location of its maximum intensity and the presence of vibrational structure (James et al., 1985). In these respects, the spectrum of RNAse-T1 is comparable to that of azurin which has a single TRP at position 48 (Burstein et al., 1977; Petrich et al., 1987). In both cases, the emission intensity maxima are significantly blue shifted relative to other single TRP proteins, being 318–320 nm in RNAse-T1 and 308 nm in azurin. Although their vibrational structure is very poorly resolved, these are the only proteins in which vibrational structure has been reasonably demonstrated. It is worthwhile to consider these fluorescence characteristics further in light of structural data provided by the simulation.

The location of a structural water (WAT-112) critically near the TRP-59 >N—H group was predicted by our simulation and confirmed by x-ray crystallography. Features of its location suggest that water may have a very long residency time at this location and that it may hydrogen-bond with atom $H_{\epsilon 1}$ of TRP-59. In contrast, there are no potential hydrogen bonds involving the TRP-48 >N—H group apparent in the x-ray structure of azurin, and the residue appears to be fully sequestered from any contact with solvent. Because hydrogen bonds shift indole emission spectra to the red (Demchenko, 1986 [pp. 34–40]), these observations suggest that the 10–12 nm difference between emission maxima of RNAse-T1 and azurin chromophores may be due to hydrogen bond formation in RNAse-T1. We note that the energy change corresponding to a 10–12 nm shift is ~3.2 kcal/mol, a value comparable in scale to the energy of a hydrogen bond.

However, hydrogen bonds in ordinary aqueous solutions tend to broaden spectral emission lines completely beyond resolution (Demchenko, 1986). If an H-bond exists between WAT-112 and TRP-59, it is apparently altered by its protein environment because we observe vestiges of distinct spectral lines in RNAse-T1. Furthermore, the degree of spectral broadening that is observed in RNAse-T1 may not be related to H-bond formation because factors other than H-bond formation must account for the similar broadening of TRP-48 in azurin.

We do not use a directional H-bond term in our dynamics potential function, and we would certainly expect such a term to affect the distribution of donor-hydrogen-acceptor geometries (Fig. 6 *a*). However we do

not know, a priori, whether such a term will shift this distribution toward or away from energetically significant H-bonds because there may be competition for any given donor or acceptor among potential H-bonding groups. For example, the peptide N—H group of TYR-68 (see Fig. 5), could conceivably compete for WAT-112 at the expense of the imino N—H group of TRP-59. Furthermore, the carbonyl group of ALA-19 is also positioned to compete with WAT-112 directly or indirectly via induced electrostatic effects. A simulation of RNAse-T1 with proper H-bond terms would therefore be of interest.

Aside from ordinary H-bond formation, there exist other bases for interaction between water and the indole >N—H group. Hager et al. (1987) show evidence for various indole derivatives that the indole N—H bond is relatively labile in the $^1L_\alpha$ excited state. Thus, charge transfer or exciplex formation with WAT-112 may occur in RNAse-T1, resulting in red shifted emission relative to TRP-48 in azurin. It is conceivable that the oxygen of WAT-112 may be unable to form optimal or long-lived H-bonds for geometric reasons and therefore may be available for other roles such as electron capture. Chaining of H-bonds via WAT-142 out to bulk solvent may add to the stabilization of charges on WAT-112.

The red shift of RNAse-T1 emission compared with azurin also correlates with a closer proximity between TRP and bulk solvent in the case of RNAse-T1. However, our simulation indicates that water which is close to or makes contact with TRP-59 is highly constrained within H-bond networks and therefore should have an attenuated dielectric screening effect. Gilson and Honig (1987) have examined the dielectric properties of bound water, finding quantitatively better correlation with experiment when bound water is modeled as a low dielectric medium. Thus, a far smaller stoke's shift for TRP-59 compared with TRP in water is certainly expected, and we might further expect that most of the energetically significant relaxation occurs between TRP-59 and nearby intrinsic protein dipoles.

The relative importance of protein versus water dipoles in the electrostatic environment of TRP-59 is difficult to assess, but their separate contributions to the effective dielectric using molecular dynamics could be estimated by altering the distribution of charge within TRP-59, repeating part of the simulation, and examining subsequent dipole reorientations. A simpler case to analyze would be that of a spherically symmetric point charge in the region of TRP-59. Neither approach, however, can adequately treat atomic polarizabilities and induced dipole shifts.

Finally, we must consider the effects of the local electrostatic potential on the absorption spectrum of TRP-59 because we might expect the fluorescence emission to shift in parallel to any shift in the absorption spectrum. Ilich et al. (1988) have attempted to calculate the effects of a single point charge on the absorption spectrum of indole. The predicted effects differ in magnitude and direction depending on the location of the charge with respect to indole, but may be sufficient to cause shifts as large as 10 nm. Electrostatic perturbation of absorption may be greater in azurin than in RNAse-T1 because we find a steeply graded electrostatic potential at TRP-48 in azurin, and a relatively bland gradient at TRP-59 in RNAse-T1 (see Fig. 10 *a–d*). It is entirely plausible that steep field gradients will modify other photophysical properties of the indole ring system, particularly as the TRP side chain moves within the gradient. For example, movement of the side chain electric dipole against a potential gradient requires energy and may be a means of nonradiative excited-state deactivation.

IV. Quantum yield

Nonradiative deactivation of excited indole molecules in gas phase occurs via intersystem crossing from the singlet to the triplet state, as well as poorly defined means of direct internal conversion to the ground state. In condensed phases, additional mechanisms of nonradiative decay are available and quantum yield becomes a function of both temperature and excitation wavelength, particularly if the solvent is polar. Indole and 3-methylindole exhibit quantum yields of ~0.40 in cyclohexane and 0.28 in water (Klein et al., 1981). The quantum yield of TRP in water is half of this value (Longworth, 1971) and diminishes a further two- to three-fold on incorporation into peptides (Werner and Forster, 1979). In this context, the quantum yield of 0.28–0.31 for TRP-59 in RNAse-T1 (Longworth, 1971; James et al., 1985) is remarkably high, and approximately equal to indole in water.

Given this high quantum yield for RNAse-T1, it is surprising that most atoms of the TRP-59 side chain frequently contact one or more highly polar groups of the nearby protein matrix in our simulation. These groups ordinarily quench fluorescence through "collisional" or "dynamic" mechanisms with low activation energies (Ricci and Nesta, 1976; Demchenko, 1986, [pp. 179–182]). The simulation results therefore imply that these mechanisms are either inoperative or very inefficient within RNAse-T1.

It appears unlikely that collisional interactions occur which are of an entirely different nature than those listed in Table 2. By this we mean that gross disruption of major secondary and tertiary structures would be necessary to bring potential quenchers such as a carboxyl group, sulfur atom, or ammonium group into contact with TRP-59. The only possible interaction appears to be with the ϵ-amino group of LYS-25 for which the crystal structure

shows a distance of 5.75 Å to atom $C_{\eta 2}$ of TRP-59 when LYS-25 lies closely apposed to the helix (our simulation used the GLN-25 isozyme). Although we would expect this side chain to protrude into the solvent and away from TRP-59 (as with GLN-25), we cannot exclude intermittent proximity to within the "sphere of influence" of the ammonium ion. If LYS-25 influences TRP-59 fluorescence, we would predict a lower quantum yield and/or shorter lifetime for the LYS-25 isozyme compared with the GLN-25 isozyme.

In addition, it may be possible for the rings of TYR-38 or TYR-68 to interact differently with the TRP-59 rings. TYR-68 is tethered to GLY-70 via H-bond throughout the trajectory, but both are members of an omega loop (Leszczynski and Rose, 1986), which exhibits large-scale motions in a vacuum simulation, and such motions could conceivably facilitate various pi-electron interactions between TYR-68 and TRP-59. For TRP-59 to interact with TYR-38 would require major structural shifts in the active site, and therefore seems less likely than TRP-59 interactions with TYR-68. A spectroscopic study of an RNAse-T1 mutant with a hydrophobic and nonaromatic residue in position 68 would likely help answer critical questions about intrinsic quenching of TRP-59.

In light of this, we must consider that the quenching efficiency of interactions listed in Table 2 may be a function not only of the nature of the interacting chemical species and their collisional frequency, but also of particular collisional geometries. The high quantum yield of TRP-59 despite the apparent high frequency of interaction between the indole moiety and potential quenchers could be explained, in part, by infrequent sampling of conformations which give rise to suitable contact geometries. This inference is consistent with the results of James et al. (1985), who demonstrated that the quantum yield and fluorescence lifetime of TRP-59 is largely temperature insensitive. These authors found a small temperature-dependent decay component with an activation energy of 30 ± 5 kJ/mol. Although this is comparable to the activation energy associated with photoionization in tryptophan, James et al. (1985) concluded that the temperature-dependent process is unlikely to be due to photoionization, because the close approach of the solvent required for this process is sterically prohibited.

James et al. (1985) speculate that the temperature-dependent decay process represents a quenching mechanism facilitated by protein mobility. On the strength of our simulation, we may elaborate on this speculation in the following way. Whereas collisional interactions with potential quenchers may occur frequently (with respect to the fluorescence lifetime) at all relevant temperatures, greater protein mobility at higher temperatures will give rise to a greater range of interaction geometries as well as more frequent interactions. Hence, particular configurations that facilitate nonradiative deactivation may arise more frequently. We note that their data demonstrate that the similarity between quantum yields for TRP-59 in RNAse-T1 and indole in water is probably coincidental, because the nonradiative deactivation of indole in water is quite temperature sensitive (reviewed by Creed, 1984) and is probably due to a photoionization decay mechanism (cf. the relative temperature insensitivity of RNAse-T1 fluorescence).

V. Lifetimes

RNAse-T1 exhibits monoexponential intensity decay at pH ≈5, but a second and shorter decay component appears at pH ≈7 or upon binding 2′-GMP (Grinvald and Stenberg, 1976; James et al., 1985; Eftink and Ghiron, 1987; Alcala et al., 1987*b*; Chen et al., 1987). In addition, a second component has been observed at pH ≈5 when the measurements are made at 40°C (MacKerrel et al., 1987; Gryczynski et al., 1988). This latter finding is consistent with the data of James et al. (1985) since from their Fig. 5, a lifetime of ≈3.4 ns may be derived for RNAse-T1 at 40°C which closely corresponds to the weighted average of the lifetimes for the free enzyme at 40°C given in Table 1 of MacKerrel et al. (1987). Although it is clear from these data that the fluorescence intensity decay of TRP-59 is sensitive to alterations in its chemical environment brought about by changes in temperature, pH, and ligand binding, these same data give us virtually no insight as to the nature of the chemical environments.

Because the fluorescence intensity of an idealized fluorophore decays monoexponentially, it has been traditional in proteins to associate each component of a multiexponential decay with the existence of a particular protein conformation. An alternative approach assumes that a large number of fluorophore environments may exist which interconvert on the fluorescence time scale giving rise to a distribution of unique lifetimes (Alcala et al., 1987*a*). Neither experimental data nor our simulation furnish us at present with a basis for choosing between models of fluorescence decay which espouse discrete versus distributed exponential decay components. Such a conclusion is unsatisfying, and may point to our failure to consider alternative explanations.

For example, if quenching of TRP-59 in RNAse-T1 is mediated by electron or proton transfer (as suggested by Chen et al., 1987), then the fluorescence lifetime may be determined by relatively long-range effects and the relevant conformation may be that of an electron or a proton accepting moiety rather than that of the fluorophore environs. Thus, if electron transfer to an imidazolium group is a principal determinant of the TRP-59 lifetime, there may be another basis for lifetime dependence on pH. If the orientation of imidazole rings are critical in this

capacity, it may help explain the effects of ligand binding on the fluorescence lifetime of RNAse-T1 in a way which is independent of the electron or proton accepting nature of the ligand.

Another alternative to consider is the formation of exciplexes between TRP-59 and water or elements of the protein matrix (Lumry and Hershberger, 1978). If a given TRP residue can form more than one exciplex, a plausible basis for multiple discrete lifetimes would exist because each exciplex may have a distinct intrinsic lifetime. However, this scenario could also be the basis for lifetime distributions because the time interval between excitation and exciplex formation is variable and the relative contributions of the uncomplexed fluorophore and the exciplex to the observed lifetime would be distributed over a range equal to the difference in lifetime between the two states. In comparison, multiple discrete lifetimes arising from a single intrinsic lifetime seems rather improbable because the rates of the nonradiative deactivation processes would have to be nonidentical, yet very similar on the fluorescence time scale purely by coincidence.

The observation that PRO-39 undergoes a rotameric transition at one point in the simulation is of interest. In the crystal structure, GLY-23 greatly retards an otherwise rapid transition from a boat to a chair configuration. It is unlikely that nonbonded interactions between TRP-59 and PRO-39 chain exclusively determine the appearance of a new and relatively short lifetime component at neutral pH, because the interaction is entirely nonpolar. More likely would be displacement of TRP-59 by PRO-39 in such a manner so as to bring about more suitable contact between TRP-59 and an intrinsic quencher. We might expect the pH-sensitive side chains of HIS-27 and HIS-40 to influence TRP-59 fluorescence by such means since both residues are spatially adjacent to PRO-39. However, there is reason to doubt whether titration of a histidine residue can be responsible for the observed pH-dependent fluorescence decay phenomena since the transition occurs at pH 6.5–7.0, and there is evidence that the pKa of these histidine residues is higher than this (Arata et al., 1979).

Because of their potential role in explaining the pH-dependent appearance of a second lifetime component, HIS-27 and HIS-40 are attractive targets for site-specific mutagenesis and/or chemical modification, along with residues with which they may potentially hydrogen bond, such as TYR-24, TYR-57, and GLU-82 in the case of HIS-27, and TYR-38 in the case of HIS-40. In addition, a simulation with protonated histidines may be of interest. Replacement of GLY-23 with ALA or VAL should be attempted in an effort to stabilize one form of PRO-39. It would be of interest to repeat the hole-burning experiment of Hershberger et al. (1980) on RNAse-T1 at acid pH and with any GLY-23 mutants that exhibited monoexponential decay at neutral pH to see if structural heterogeneity by this measure is present only when there is multiexponential fluorescence decay. It will likely be difficult to mutate the potentially critical residues PRO-39 or PRO-60 conservatively such that overall protein conformation and enzyme activity is preserved.

VI. Extrinsic quenching

In lieu of modeling specific quenching molecules, we have examined water behavior as a first approximation to the behavior of a class of hydrogen bonding quenchers which includes acrylamide and trichloroethanol. Our simulation suggests that TRP-59 is rarely, if ever, completely shielded from solvent water by protein matrix. The frequency of contact between water and TRP-59 is nonetheless lower than we might expect, due in part to the energetic cost associated with the breaking of hydrogen bonds to other solvent molecules. Acrylamide and trichloroethanol each have nonpolar and polar aspects wherein we might expect the polar ends to preferentially orient toward solvent and away from TRP-59. From this orientation the quenching event may require the breaking of H-bonds and reorientation of the polar end toward TRP-59 if quenching requires contact with the polar moiety.

These observations illustrate features of the "gated" model of fluorescence quenching and particularly support the transition state approach (Somogyi et al., 1986). However, the transition state (using water-TRP contact as a model for the quenching event) is seen to be rather frequently sampled late in the trajectory. Given that acrylamide is assumed to have a high quenching efficiency, contacts between acrylamide and TRP of such frequency (several per picosecond) would appear as "static" quenching, a feature not evident from Stern-Volmer plots of RNAse-T1 fluorescence quenching by acrylamide (Eftink and Ghiron, 1976).

The limited accessibility of TRP-59 in RNAse-T1 to contact quenchers as described above has interesting implications when one considers the use of such quenchers to determine limiting anisotropies. In RNAse-T1, the limiting anisotropy of TRP-59 is nearly equivalent to that of TRP in vitrified solvent (Lakowicz et al., 1983; Ghiron and Longworth, 1979), indicating that TRP-59 is virtually immobilized within its protein matrix. To facilitate contact between molecular oxygen or acrylamide and a non-edge aspect of the rings (i.e., a ring face), extensive movements on the part of residues adjacent to TRP-59 would have to occur on a time scale which is short relative to the fluorescence lifetime. Inspection of the RNAse-T1 crystal structure and our dynamics simulation indicates that the molecular motions which would be needed to

allow such events would also permit significant rotational excursions of the TRP-59 side chain. Therefore, because these motions are not observed, quenching must occur via contact between the quencher and the extremely limited solvent-accessible "edge" aspect of the fluorophore, i.e., atoms $H_{\eta 2}$ and $H_{\zeta 2}$.

We do not know exactly how close so-called "collisional" quenchers must be to a fluorophore to effect quenching, the sphere of action concept notwithstanding (reviewed by Eftink and Ghiron, 1976; Lakowicz, 1983). If quenching events may be mediated over distances that exceed the sum of the atomic VDW radii, our conclusion that quenching is mediated via interaction with aromatic ring hydrogens may not be valid. On the other hand, our simulation may be of insufficient duration or accuracy to reveal protein motions which preclude ring librations but yet allow quencher contact with other aspects of the TRP rings. In any case, we have not detected slow motions of TRP-59 or adjacent residues that would suggest that patterns of motion relevant to the quenching process would be substantially different at times beyond 50 ps.

If our conclusions regarding orientational specificity of TRP-59 quenching are correct as expressed above, we can interpret the high efficiency of TRP-59 quenching by oxygen in terms of its symmetry. The fact that molecular oxygen exhibits axial and reflection symmetry means that there are relatively few possible interaction geometries between it and a fluorophore. Hence, given any collision between oxygen and TRP, an effective interaction has a high probability of occurring. Furthermore, by virtue of its hydrophobicity and molecular dimensions, oxygen may preferentially displace water and have a prolonged residency time in the surface pit adjacent to TRP-59 due to "solvent cage" effects. This speculation is supported in the case of acrylamide by our solvent-accessible surface area calculations which indicate that TRP-59 represents $5 \div 4{,}000 = 0.00125$ of the protein surface, yet acrylamide quenches with a bimolecular quenching constant that is as much as 10% of the diffusion-limited value (Eftink and Ghiron, 1975). Thus, "solvent cage" effects or specific interactions such as hydrogen bonding to the peptide hydrogen of TYR-68 may be contributing factors to the high apparent efficiency of RNAse-T1 quenching by acrylamide.

The accuracy of these inferences are to a considerable extent contingent on the precise mechanism by which fluorescence quenching occurs. The Stern-Volmer formalism, based as it is on the Smoluchowski relationship, implicitly assumes isotropic reaction conditions, i.e., that quencher and fluorophore have equal probability of interaction in all directions. This assumption is useful as a first approximation, but the location and apparently limited exposure of the TRP-59 rings in RNAse-T1 effectively precludes isotropic interaction with quenching agents. Under such circumstances, we conclude that quenching efficiency may be a function of interaction geometry and, accordingly, the symmetry of both fluorophore and quencher.

VII. General conclusions

We have used molecular dynamics to investigate possible correlations between protein fluorescence and structure. Our specific conclusions will not be repeated here because they are summarized in the abstract, but in general, the approach is useful for generating hypotheses and suggesting specific experimental approaches for testing them. Although molecular dynamics simulations of proteins are encumbered with severe limitations and approximations, this approach reveals many often subtle dynamic features of the fluorophore environment which would be difficult if not impossible to anticipate solely from the specific structural features revealed by x-ray crystallography.

It is important that simulations of additional single TRP proteins be conducted. By comparatively examining TRP residues with substantially different spectral properties it is expected that determinants of protein fluorescence behavior will be uncovered and the use of TRP as a probe of protein structure and dynamics can be advanced. Furthermore, such studies enable further testing and refining of molecular dynamics methodology insofar as they offer one of the few opportunities to directly compare simulation results with experiment. Proteins such as phospholipase A2, azurin, staphylococcal nuclease, and proteinase A (from *S. griseus*) are particulary attractive for these purposes, since they are each of tractable size and have known crystal structures. We are encouraged by preliminary data (not shown) from a 110-ps stochastic boundary simulation of phospholipase A2 in which TRP-3 lies fully exposed to solvent on the protein surface. As with RNAse-T1, the simulated anisotropy decay and the experimental limiting anisotropy are in excellent agreement.

The authors would like to thank The Minnesota Supercomputer Institute for computational support at the Minnesota Supercomputer Center and the Ahmanson Foundation for funds to purchase an Evans and Sutherland graphics facility. This work was supported by GM34847 and presented at the meeting of the Biophysical Society, 28 February–3 March 1988.

Received for publication 13 September 1988 and in final form 8 March 1989.

REFERENCES

Adman, E. T., and L. H. Jensen. 1981. Structural Features of Azurin at 2.7 Angstroms Resolution. *Isr. J. Chem.* 21:8.

Alcala, J. R., E. Gratton, and F. G. Prendergast. 1987*a*. Fluorescence lifetime distributions in proteins. *Biophys. J.* 51:597–604.

Alcala, J. R., E. Gratton, and F. G. Prendergast. 1987*b*. Interpretation of fluorescence decays in proteins using continuous lifetime distributions. *Biophys. J.* 51:925–936.

Arata, Y., S. Kimura, H. Matsuo, and K. Narita. 1979. Proton and phosphorus nuclear magnetic resonance studies of ribonuclease-T1. *Biochemistry.* 18:18–24.

Arni, R., U. Heinemann, M. Maslowska, R. Tokuoka, and W. Saenger. 1987. Restrained least-squares refinement of the crystal structure of the ribonuclease-T1:2'guanylic acid complex at 1.9 Å resolution. *Acta Crystallogr. Sect. B Struct. Crystallogr. Cryst. Chem.* 43:548–554.

Axelsen, P. H., C. Haydock, and F. G. Prendergast. 1988. Molecular dynamics of tryptophan in ribonuclease-T1. I. Simulation strategies and fluorescence anisotrophy decay. *Biophys. J.* 54:249–258.

Bash, P. A., U. C. Singh, F. K. Brown, R. Langridge, and P. A. Kollman. 1987. Calculation of the relative change of binding free energy of a protein-inhibitor complex. *Science (Wash. DC).* 235:574–576.

Beechem, J. M., and L. Brand. 1985. Time-resolved fluorescence of proteins. *Annu. Rev. Biochem.* 54:43–71.

Bernstein, F. C., T. F. Keotzle, G. J. B. Williams, E. F. Meyer, M. D. Brice, J. R. Rodgers, O. Kennard, T. Shimanouchi, and M. Tasumi. 1977. The Brookhaven protein data bank. *J. Mol. Biol.* 112:535–542.

Brooks B. R., R. E. Bruccoleri, B. D. Olafson, D. J. States, S. Swaminathan, and M. Karplus. 1983. CHARMM: a program for macromolecular energy, minimization, and dynamics calculations. *J. Comp. Chem.* 4:187–217.

Burstein, E. A., N. S. Vedenkina, and M. N. Ivkova. 1973. Fluorescence and the location of tryptophan residues in protein molecules. *Photochem. Photobiol.* 18:263–279.

Burstein, E. A., E. A. Permyakov, V. A. Yashin, S. A. Burkhanov, and A. F. Agro. 1977. The fine structure of luminescence spectra of azurin. *Biochim. Biophys. Acta.* 491:155–159.

Chen, L. X.-Q., J. W. Longworth, and G. R. Fleming. 1987. Picosecond time-resolved fluorescence of ribonuclease-T1. A pH and substrate analogue binding study. *Biophys. J.* 51:865–873.

Chen, L. X.-Q., R. A. Engh, and G. R. Fleming, 1988*a*. Reorientation of tryptophan and simple peptides. Onset of internal flexibility and comparison with molecular dynamics simulation. *J. Phys. Chem.* 92:4811–4816.

Chen, L. X.-Q., R. A. Engh, A. T. Brunger, D. T. Nguyen, M. Karplus, and G. R. Fleming. 1988*b*. Dynamics simulation studies of apoazurin of *Alcaligenes denitrificans*. *Biochemistry.* 88:6908–6920.

Connolly, M. L. 1983. Solvent-accessible surfaces of proteins and nucleic acids. *Science (Wash. DC).* 221:709–713.

Cotton, F. A., E. E. Hazen, Jr., and M. J. Legg. 1979. Staphylococcal nuclease. Proposed mechanism of action based on structure of enzyme-thymidine 3',5'-biphosphate-calcium ion complex at 1.5 Å resolution. *Proc. Natl. Acad. Sci. USA.* 76:2551–2555.

Creed, D. 1984. The photophysics and photochemistry of the near-UV absorbing amino acids. I. Tryptophan and its simple derivatives. *Photochem. Photobiol.* 39:537–562.

Demchenko, A. P. 1986. Ultraviolet Spectroscopy of Proteins. Springer-Verlag, Berlin.

Eftink, M., and C. A. Ghiron. 1975. Dynamics of a protein matrix revealed by fluorescence quenching. *Proc. Natl. Acad. Sci. USA* 72:3290–3294.

Eftink, M., and C. A. Ghiron. 1976. Exposure of tryptophanyl residues in proteins. Quantitative determination by fluorescence quenching studies. *Biochemistry.* 15:672–680.

Eftink, M. 1983 Quenching-resolved emission anisotropy studies with single and multitryptophan-containing proteins. *Biophys. J.* 43:323–334.

Eftink, M., and C. A. Ghiron. 1987. Frequency domain measurements of the fluorescence lifetime of ribonuclease-T1. *Biophys. J.* 52:467–473.

Ghiron, C. A., and J. W. Longworth. 1979. Transfer of singlet energy within trypsin. *Biochemistry.* 18:3828–3832.

Ghosh, I., and J. A. McCammon. 1987. Sidechain rotational isomerization on proteins. Dynamic simulation with solvent surroundings. *Biophys. J.* 51:637–641.

Gilson, M. K., and B. H. Honig. 1987. Calculation of Electrostatic potentials in an enzyme active site. *Nature (Lond.)* 330:84–86.

Grinvald, A., and I. Z. Stenberg. 1976. The fluorescence decay of tryptophan residues in native and denatured proteins. *Biochim. Biophys. Acta.* 427:663–678.

Gryczynski, I., M. Eftink, and J. R. Lakowicz. 1988. Conformational heterogeneity in proteins as an origin of heterogeneous fluorescence decays, illustrated by native and denatured ribonuclease T1. *Biochim. Biophys. Acta* 954:244–252.

Hager, J. W., D. R. Demmer, and S. C. Wallace. 1987. Electronic spectra of jet-cooled indoles: evidence for the ^1L_a state. *J. Phys. Chem.* 91:1375–1382.

Heinemann, U., and W. Saenger. 1982. Specific protein-nucleic acid recognition in ribonuclease-T1-2'-guanylic acid complex: an x-ray study. *Nature (Lond.)* 299:27–31.

Henry, E. R., and R. M. Hochstrasser. 1987. Molecular dynamics simulations of fluorescence polarization of tryptophans in myoglobin. *Proc. Natl. Acad. Sci. USA* 84:6142–6146.

Hershberger, M. V., A. H. Maki, and W. C. Galley. 1980. Phosphorescence and optically detected magnetic resonance studies of a class of anomalous tryptophan residues in globular proteins. *Biochemistry.* 19:2204–2209.

Ilich, P., P. H. Axelsen, and F. G. Prendergast. 1988. Electronic transitions in molecules in static external fields. I. Indole and TRP-59 in Ribonuclease-T1. *Biophys. Chem.* 29:341–349.

James, D. R., D. R. Demmer, R. P. Steer, and R. E. Verrall. 1985. Fluorescence lifetime quenching and anisotropy studies of ribonuclease-T1. *Biochemistry.* 24:5517–5526.

Klein, R., I. Tatischeff, M. Bazin, and R. Santus. 1981. Photophysics of indole. Comparative study of quenching, solvent, and temperature effects by laser flash photolysis and fluorescence. *J. Phys. Chem.* 85:670–677.

Lakowicz, J. R. 1983. Principles of Fluorescence Spectroscopy. Plenum Publishing Corp., New York.

Lakowicz, J. R., B. P. Maliwal, H. Cherek, and A. Balter. 1983. Rotational freedom of tryptophan residues in proteins and peptides. *Biochemistry.* 22:1741–1752.

Lakowicz, J. R., G. Laczko, I. Gryczynski, and H. Cherek. 1986. Measurement of subnanosecond anisotropy decays of protein fluorescence using frequency-domain fluorometry. *J. Biol. Chem.* 261:2240–2245.

Lakowicz, J. R., G. Laczko, and I. Gryczynski. 1987. Picosecond resolution of tyrosine fluorescence and anisotropy decays by 2-GHz frequency-domain fluorometry. *Biochemistry.* 26:82–90.

Lee, B., and F. M. Richards. 1971. The interpretation of protein structures: estimation of static accessibility. *J. Mol. Biol.* 55:379–400.

Leszczynski, J. F., and G. D. Rose. 1986. Loops in globular proteins: a novel category of secondary structure. *Science (Wash. DC)*. 234:849–855.

Longworth, J. W. 1971. Luminescence of polypeptides and proteins. *In* Excited States of Proteins and Nucleic Acids. R. F. Steiner, and I. Weinryb, editors. Plenum Publishing Corp., New York.

Lumry, R. and M. Hershberger. 1978. Status of indole photochemistry with special reference to biological applications. *Photochem. Photobiol.* 27:819–840.

MacKerrell, A. D., Jr., R. Rigler, L. Nilsson, U. Hahn, and W. Saenger. 1987. A time-resolved fluorescence, energetic, and molecular dynamics study of ribonuclease-T1. *Biophys. Chem.* 26:247–261.

MacKerrell, R., Jr., A. D. Nilsson, R. Rigler, and W. Saenger. 1988. Molecular dynamics simulations of ribonuclease-T1: analysis of the effect of solvent on the structure, fluctuations, and active site of the free enzyme. *Biochemistry*. 27:4547–4556.

Petrich, J. W., J. W. Longworth, and G. R. Fleming. 1987. Internal motion and electron transfer in proteins: a picosecond fluorescence study of three homologous azurins. *Biochemistry*. 26:2711–2722.

Politzer, P., and D. G. Truhlar, editors. 1981. Chemical Applications of Atomic and Molecular Electrostatic Potentials. Plenum Publishing Corp., New York.

Ricci, R. W., and J. M. Nesta. 1976. Inter- and intramolecular quenching of indole fluorescence by carbonyl compounds. *J. Phys. Chem.* 80:974–980.

Ringe, E., and G. A. Petsko. 1985. Mapping protein dynamics by x-ray diffraction. *Prog. Biophys. Mol. Biol.* 45:197–235.

Rizzo, T. R., Y. D. Park, L. A. Peteanu, and D. H. Levy. 1986. The electronic spectrum of the amino acid tryptophan in the gas phase. *J. Phys. Chem.* 84:2534–2541.

Russel, S. T., and A. Warshel. 1985. Calculation of electrostatic energies in proteins. The energetics of ionized groups in bovine pancreatic trypsin inhibitor. *J. Mol. Biol.* 185:389–404.

Somogyi, B., J. A. Norman, and A. Rosenberg. 1986. Gated quenching of intrinsic fluorescence and phosphorescence of globular proteins. An extended model. *Biophys. J.* 50:55–61.

Tanaka, I., T. Kozima, T. Ashida, N. Tanaka, and M. Kakudo. 1977. Benzyloxycarbonylglycyl-L-proline. *Acta Crystallogr. Sect. B Struct. Crystallogr. Cryst. Chem.* 33:116–119.

Van Belle, D., I. Couplet, M. Prevost, and S. J. Wodak. 1987. Calculations of electrostatic properties in proteins. Analysis of contributions from induced protein dipoles. *J. Mol. Biol.* 198:721–735.

Werner, T. C., and L. S. Forster. 1979. The fluorescence of tryptophyl peptides. *Photochem. Photobiol.* 29:905–914.